Title

Nanocarrier Co-formulation for Delivery of a TLR7 Agonist plus an Immunogenic Cell Death Stimulus Triggers Effective Pancreatic Cancer Chemo-immunotherapy

Journal

ACS Nano, 16(8)

ISSN

1936-0851

Authors

Luo, Lijia
Wang, Xiang
Liao, Yu-Pei
et al.

Publication Date

2022-08-23

DOI

10.1021/acsnano.2c06300

Peer reviewed

HHS Public Access

Author manuscript

ACS Nano. Author manuscript; available in PMC 2023 August 23.

Published in final edited form as:

ACS Nano. 2022 August 23; 16(8): 13168–13182. doi:10.1021/acsnano.2c06300.

Nanocarrier Co-formulation for Delivery of a TLR7 Agonist plus an Immunogenic Cell Death Stimulus Triggers Effective Pancreatic Cancer Chemoimmunotherapy

Lijia Luo[†,‡], **Xiang Wang**[†,‡], **Yu-Pei Liao**[†], **Chong Hyun Chang**[‡], **Andre E. Nel**[*,†,‡]

[†]Division of Nanomedicine, Department of Medicine, University of California, Los Angeles, California 90095, United States

[‡]California NanoSystems Institute, University of California, Los Angeles, California 90095, United States

Abstract

Although toll-like receptor (TLR) agonists hold great promise as immune modulators for reprogramming the suppressive immune landscape in pancreatic ductal adenocarcinoma (PDAC), their use is limited by poor pharmacokinetics (PK) and off-target systemic inflammatory effects. To overcome these challenges as well as to attain drug synergy, we developed a lipid bilayer (LB)-coated mesoporous silica nanoparticle (silicasome) platform for co-delivery of the TLR7/8 agonist, 3M-052, with the immunogenic chemotherapeutic agent, irinotecan. This was accomplished by incorporating the C18 lipid tail of 3M-052 in the coated LB, also useful for irinotecan remote loading in the porous interior. Not only did the co-formulated carrier improve PK, but strengthened the irinotecan-induced immunogenic cell death (ICD) response by 3M-052-mediated dendritic cell activation at the tumor site as well as participating lymph nodes. The accompanying increase in $CD8^+$ T-cell infiltration along with a reduced number of regulatory T-cells was associated with tumor shrinkage and metastasis disappearance in subcutaneous and orthotopic KRAS-mediated pancreatic carcinoma (KPC) tumor models. Moreover, this therapeutic outcome was accomplished without drug or nanocarrier toxicity. All considered, dual-delivery strategies that combine chemo-immunotherapy with co-formulated TLR agonists or other lipid-soluble immune modulators predict successful intervention in heterogeneous PDAC immune landscapes.

Graphical Abstract

[*]**Corresponding Author:** anel@mednet.ucla.edu.

Supporting Information

The Supporting Information is available free of charge on the ACS Publications website.

Additional figures and table, e.g., MTT, flow cytometry, body weight, and representative IHC staining, as described in the text (PDF).

The authors declare the following competing financial interest(s): Andre E. Nel is cofounder and equity holder in Westwood Biosciences Inc. and NAMMI Therapeutics. Nel also serves on the Board for Westwood Biosciences, Inc.

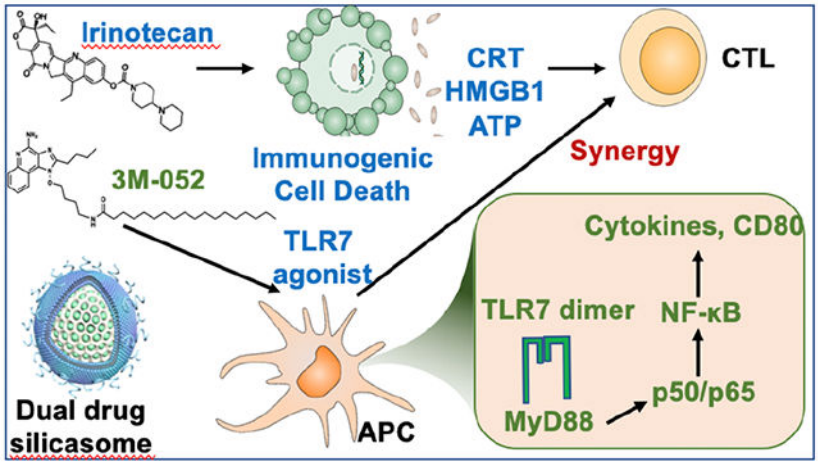

We developed a co-formulated drug carrier that incorporates a TLR7 agonist in the lipid bilayer of silicasomes, which also allow remote import of the chemo-immunotherapeutic agent, irinotecan, through the bilayer. The generation of an immunogenic cell death response by irinotecan synergizes with dendritic cell activation by 3M-052, resulting in a robust immune response in a pancreatic ductal adenocarcinoma immune landscape.

Keywords

dual drug silicasome; TLR agonists; 3M-052; pancreatic cancer; dendritic cells; chemo-immunotherapy

Pancreatic ductal adenocarcinoma (PDAC) is the third leading cause of cancer death in the United States, with a five-year survival rate of ~11%.[1,2] The poor prognosis is due to late clinical presentation, as well as interference in drug delivery and drug resistance by an abundant dysplastic stroma.[3] To improve the pharmacokinetics (PK) of drug delivery, a number of nanocarriers have been introduced for PDAC treatment recently, including the irinotecan-delivering liposome, Onivyde, and an albumin-paclitaxel nanocarrier, nab-paclitaxel (Abraxane).[4,5] While the principal consideration for nab-paclitaxel development was to overcome the toxicity of an incipient, Onivyde was developed to improve the efficacy of combination chemotherapy in patients with metastatic disease and who failed to respond to gemcitabine treatment. More recently, the pegylated irinotecan liposome was also approved as first-line therapy for untreated, locally-advanced, metastatic disease in combination with oxaliplatin, 5-fluorouracil, and leucovorin. However, while Onivyde improved therapeutic efficacy, the drug received a black box warning for severe diarrhea and neutropenia, most likely related to carrier leakage from the impact of plasma proteins, complement and circulatory shear forces on the intactness of the lipid bilayer (LB).[4] These shortcomings were instrumental in the development of silicasomes, which make use of a supported LB for coating of mesoporous silica nanoparticles (MSNPs).[6,7] Not only is the supported LB more stable, but also allows irinotecan remote loading and high drug import into the porous interior. This allowed us to accomplish improved irinotecan delivery to orthotopic KRAS-dependent pancreatic cancer (KPC) tumors compared to Onivyde, in

addition to demonstrating the absence of bone marrow toxicity, blunting of intestinal villi, and hepatotoxicity, which are seen during treatment with free or liposomal irinotecan.[8]

An exciting recent advance for silicasome use and irinotecan delivery is the demonstration that this chemo agent also induced immunogenic cell death (ICD), in addition to its role as a topoisomerase I inhibitor.[9] The robust induction of ICD was explained by a collateral irinotecan effect on lysosomal alkalization, leading to interference in autophagy flux and generation of endoplasmic reticulum stress.[10,11] This culminates in a robust generation of immune danger signals to assist the specialized cell death response, which promotes dying cancer cell uptake by bystander antigen-presenting cells (APCs). This action involves calreticulin (CRT) expression on the dying tumor cell surface, further assisted by high mobility group protein B1 (HMGB1) and ATP release, which function as adjuvant stimuli to promote dendritic cell (DC) activation and maturation.[12,13] The ICD process can be likened to an endogenous tumor vaccination response, allowing tumor antigen presentation to naïve T-cells by DC in secondary lymphoid organs (lymph nodes and spleen). The activated $CD8^+$ cytotoxic T-cells (CTLs) return to the primary tumor site to complete the cancer immunity cycle.[14]

Not only did irinotecan induce an ICD response, but could also be seen to promote PD-L1 expression as a consequence of endoplasmic reticulum stress.[9] This allowed us to strengthen the ICD response by co-administration of a monoclonal antibody that blocks PD-L1 binding to PD-1. The combinatorial effect raised the possibility of using the multifunctional features of the silicasome to co-formulate immunomodulators, selected to intervene in a host of immune challenges in the PDAC immune landscape, resulting from the paucity of neoantigens, poor recruitment of APC, checkpoint receptor-mediated immune escape and immune suppressive cellular components in the tumor microenvironment (TME).[15] A facile design emerging from this thinking was to use the packaging space for incorporation of ICD-inducing chemo agents (such as irinotecan) into the particle pores, while including synthetic lipid immunomodulators such as toll-like receptor (TLR) agonists or lipid-conjugated prodrugs into the LB to deliver adjuvant stimuli or interfere in immune checkpoint pathways (Figure 1).[15]

The ubiquitously expressed toll-like receptor (TLR) family functions as pattern recognition receptors (PRRs), capable of activating the innate immune system in response to pathogen-associated molecular patterns (PAMPs) or damage-associated molecular patterns (DAMPs).[16,17] All TLRs share a typical structural motif in the form of leucine-rich repeats, which upon dimerization by cognate ligands, induce recruitment of adapter and signaling molecules providing transcriptional activation in innate immune cells.[18–20] For instance, TLR7, an endosomal-expressed receptor, is capable of sensing viral single-stranded (ss) RNA, leading to NF-κB/AP1 and IRF-mediated expression of type I IFNs, pro-inflammatory cytokines, and co-stimulatory molecules (e.g., CD80 and CD86) in antigen presenting cells (APC), including dendritic cells.[21] This introduces TLR7 and a closely related endosomal homolog, TLR8, as attractive therapeutically assessable immune modulators for boosting innate immunity in the context of infectious disease and tumor immune landscapes. Historically, the first patent filing was for a drug known as imiquimod (a.k.a. R837) to treat genital warts and basal cell carcinomas, followed

by introduction of resiquimod (R848), which is 10-fold to 100-fold times more potent than R837.[22,23] However, while these agents triggered robust immune activation during conducting of clinical trials, a major setback was the occurrence of systemic on-target/off-tumor inflammatory reactions.[20,24] Consequently, drug advancement focused on local or encapsulated drug delivery. For instance, 3M-052, an imidazoquinoline compound linked to a C18 lipid tail, was used to construct liposomal, polylactic co-glycolic acid (PLGA) and small lipid nanoparticles, to provide adjuvant stimuli for attempts at infectious disease vaccination.[25–28] In addition, the small molecule TLR7 agonist, 1V209, was used for cholesterol conjugation (1V209-Cho) and incorporation into a nanocarrier capable of reaching lymph nodes and boosting immunotherapy responses in CT26 colorectal, 4T1 breast cancer, and Pan02 PDAC tumor models.[29] This included demonstration that that improved DC activation leads to the boosting of immune responses without systemic side effects.

Based on this background as well as the awareness of poor dendritic cell function in human and murine PDAC microenvironments, we hypothesized that the 3M-052 lipid tail would be ideal for LB incorporation of irinotecan-delivering silicasomes, with the possibility of strengthening the chemoimmunotherapy response by DC activation. To test this hypothesis, we developed a method for 3M-052 incorporation into the LB being coated onto the surface of MSNP. The carrier was subsequently used for irinotecan remote loading before intravenous (IV) injection in PDAC tumor-bearing mice. We demonstrate generation of a synergistic anti-PDAC immune response by improved drug delivery, including through boosting of APC activity that also involve regional lymph nodes. This is in keeping with our blueprint for synergistic nanocarriers to interfere in heterogeneous immune landscapes.[15]

Results and Discussion

Development of Dual-drug Silicasomes that deliver Irinotecan plus 3M-052

The envisaged design principle for accomplishing a co-formulated silicasome carrier requires remote loading of irinotecan (IRIN) into the porous packaging space of the silicasome using a protonating agent, while incorporating 3M-052 (a.k.a. Telratolimod) into the lipid bilayer (LB) (Figure 1). To develop an appropriate bilayer composition, we experimented with a series of lipid biofilms to determine whether 3M-052 can be stably incorporated into a LB. The optimal lipid bilayer composition was achieved with DSPC/Chol/DSPE-PEG2000/3M-052 in the molar ratio of 55.5:38.5:2.7:3.3); this yielded liposomes with average size of 135.8 ± 2.2 nm and a 3M-052 loading capacity of 1.5% (Figure S1). We also demonstrated achievement of an IRIN remote loading capacity of 18.6% through the use of $(NH_4)_2SO_4$ as trapping agent. Additional physicochemical characteristics of this carrier, designated 3M-liposome-IRIN, appear in Figure S1.

Successful establishment of a 3M-052 lipid bilayer allowed us to proceed with silicasome construction. Controlled synthesis of spherical MSNPs was accomplished using a heated CTAC solution for TEOS addition, as previously described by us.[6–8] The particles were soaked in a trapping agent, TEA_8SOS, before sonicating in a lipid solution of similar composition as described above (Figure 2A). Following removal of free TEA_8SOS, IRIN remote loading and silicasome purification was accomplished as previously described by

us.[8] This yielded a carrier, designated as 3M-silicasome-IR (also abbreviated as 3M-Si-IR). As a control, we also prepared a nanocarrier loaded with 3M-052 only, designated a 3M-silicasome or 3M-Si. Cryo-electron microscopy (CyroEM) of both carriers confirmed the presence of MSNPs with a worm-like porous structure, coated with an intact LB (Figures 2B and C). Hydrodynamic size measurement showed sizes of 112.2 ± 1.0 and 127.0±2.9 nm for the 3M-silicasome and 3M-silicasome-IR carriers, respectively (Figure 2D). While a loading capacity of 2.1% could be achieved for 3M-052 in the single-drug carrier, the proportional loading capacity was reduced to 1.5% in the dual-delivery carrier, after consideration of the IRIN incorporation (at a loading capacity of 38%).

Demonstration of TLR7/8 Activation by Encapsulated 3M-052 in cellular studies

Both the TLR7 and TLR8 receptors are widely expressed in innate immune cells, including DC and macrophages. Their endosomal localization allows intracellular sensing of single-stranded viral RNA, leading to receptor dimerization and triggering of transcriptional activation pathways involved in DC and macrophage activation and maturation (Figure 3A). More specifically, TLR7 and TLR8 dimerization leads to the recruitment of the adaptor protein, myeloid differentiation primary response 88 (MyD88), which triggers NF-κB/AP-1 mediated signaling cascades that induce production of pro-inflammatory cytokines such as IL-6, IL-12p40, and TNF-α.

To confirm intracellular delivery and attainment of a TLR7 agonist effect by the 3M-silicasome, we used a commercially available HEK-Blue™ cell line, which expresses the murine TLR7 gene and an NF-κB/AP-1-responsive SEAP (secreted embryonic alkaline phosphatase) reporter gene (Figure 3A). This allows detection of SEAP levels in the culture medium of the cells exposed to 0.01 to 10 μM free R848 (positive control), free 3M-052, or the 3M-silicasome for 20 h (Figure 3B). Quantification of SEAP levels, using the HEK-Blue™ Detection kit, demonstrated differential dose-response relationships for R848 versus free and encapsulated 3M-052 at lower dose range, but became equivocal at 10 μM.

Having confirmed effective intracellular delivery of the TLR7 agonist, the next task was to determine the effect of the 3M-silicasome in the *ex vivo* activation of macrophages and DCs. These assays were performed in RAW264.7 macrophages and murine bone marrow-derived dendritic cells (BMDCs). RAW264.7 and BMDCs were treated with 10 μM each of R848 (positive control), free 3M-052, or the 3M-silicasome for 21 hours before assessing CD80 expression (Figures 3C and E). The flow cytometry assessment demonstrated a significant increase in cell surface expression of a maturation marker, regulated by NF-κB and AP-1 response elements. We also quantified the release of two key pro-inflammatory cytokines, by ELISA in the same cell types, using similar stimuli. This confirmed significant cytokine release into the culture supernatants, demonstrating higher responsiveness to free and encapsulated 3M-052 than for R848 ((Figures 3D and F). These results are in accordance with previous studies. For instance, Wightman's group has demonstrated that 3M-052 induced higher expression of TNF-α in vitro compared to R848.[25] Similarly, Pulendran's group demonstrated a stronger immune response triggered by 3M-052 compared to TLR-7/8 (R848) plus TLR-4 (MPL) combined.[28]

To confirm cellular uptake of the 3M-silicasome in RAW264.7 and BMDC, a cellular study was performed, using a DiD-labeled 3M-silicasome carrier with the characteristics shown in Figure S2A. Flow cytometry was used to assess cellular fluorescence following incubation with a carrier dose range delivering incremental amounts of encapsulated 3M-052 (Figures S2B and C). This demonstrated a dose-related increase in cellular fluorescence with almost all cells engaging in particle association. There was no evidence of toxicity in response to encapsulated 3M-052 in RAW267.4 cells, as well as a pancreatic cancer cell line (KPC) derived from the genetically-engineered KRAS mouse pancreas cancer model (Pdx1-cre/LSL-Kras G12D/p53R172H) (Figures S3A and B). To assess the impact of IRIN delivery on KPC cells, they were exposed to a wide dose range of free and encapsulated IRIN for 48 h (Figure S3C). This demonstrated dose-dependent cytotoxicity, with a steeper decline in viability in response to the free drug (Figure S3C). Noteworthy, we have previously demonstrated that the KPC cell death response to IRIN involves a combination of nuclear damage (topoisomerase 1 inhibition) plus triggering of an endoplasmic reticulum (ER) stress response (Figure S3D).[11] Collectively, this culminates in an ICD response, which is characterized by calreticulin (CRT) expression on the cell surface, as well as HMGB1 and ATP release from the dying cells (Figure S3D). CRT acts as a “eat-me” signal for APC processing while HMGB1 and ATP act as adjuvants for APC activation and maturation.[12,13] *In vivo* studies will further demonstrate the relevance of the mode of cell death to immune response boosting by 3M-052.

Demonstration of Carrier Therapeutic Efficacy and Immune Activation in a Subcutaneous KPC Tumor Model

KPC cells were subcutaneously injected into the right flank of female B6129SF1/J mice for *in vivo* experimentation. Following tumor growth to ~100 mm^3, groups of 6–7 animals received IV injection of saline, free 3M-052 (2 mg/kg), free IRIN (40 mg/kg), 3M-silicasome (3M-052, 2 mg/kg) and 3M-silicasome-IR (3M-052, 2 mg/kg; IRIN, 40 mg/kg) every 3 or 4 days for a total of four administrations(Figure 4A). Subcutaneous tumor sizes were monitored every 2 days. While all treatment modalities significantly impacted the tumor volumes at the harvesting stage compared to saline ($p < 0.001$), the effects of free 3M-052 and free IRIN were significantly reduced compared to treatment with single-drug or dual-drug silicasomes ($p < 0.01$) (Figure 4B). Moreover, tumor volume reduction in mice treated with the dual-delivery carrier was significantly less ($p < 0.05$) than for the 3M-silicasome. These findings were further corroborated by capture of photographic images displaying tumor size at the time of harvest (Figure 4C), as well as displaying the growth kinetics of individual tumors, displayed as spaghetti plots (Figure 4D). Differences in the response outcome between free 3M-052 and the 3M-silicasome suggested that encapsulated delivery is more efficacious in promoting the anti-PDAC immune response at the primary tumor site.

In order to investigate the specifics of the immune response induced at the primary cancer site, tumors were harvested from sacrificed animals on day 21 for performance of immunohistochemistry (IHC) analysis. We looked at the appearance of $CD8^+$ T-cells, demonstrating that both the 3M-silicasome-IR as well as the 3M-silicasomes could induce significant $CD8^+$ CTL recruitment compared to free IRIN or free 3M-052 (Figure 5A).

Representative IHC images are shown underneath the graphic, with the comprehensive data panel appearing in Figure S4 online. We also performed IHC staining to assess the presence of FoxP3$^+$ expression on regulatory T-cells (Tregs), which contribute the to immune suppressive PDAC landscape.[30–32] Quantification of FoxP3$^+$ cell number demonstrated a highly significant reduction of this marker for all treatment modalities, the most robust contribution being that of the 3M-silicasome-IR (Figures 5A and S4). Additional display of the number of CD8$^+$ *vs.* FoxP3$^+$ T-cells, reflected as a ratio, confirmed that the biggest ratio increase occurred in the dual-delivery carrier compared to other treatment modalities. The magnitude of change is in favor of a synergistic response generation by co-delivery of irinotecan with the TLR7 agonist.

Subcutaneous tumor implantation in the rear animal flank allows lymphatic drainage to the regional inguinal lymph nodes (LNs), which were harvested to assess therapeutic impact on LN-resident dendritic cells (LN-DCs). This reasoning is premised on the possibility that LN participation in the cancer immunity cycle may be able to strengthen the ICD response by increased recruitment of newly-activated cytotoxic T-cells back to the principal tumor site. Following inguinal LN harvesting and cellular release, initial flow cytometry gating selected singlet live cells (Figure S5). Further gating on the CD11c$^+$/CD45$^+$ DC subset was used to quantify CD80 and CD86 expression, representative of the surface receptors on an activated DC subset that participate in T-cell activation. Flow analysis demonstrated an increase in the percentage of CD45$^+$/CD11c$^+$ LN-DCs in response to free or encapsulated 3M-052 delivery (single and dual-drug carriers), compared to saline and free IRIN (Figure 5B). Moreover, while CD80 and CD86 expression were up-regulated in response to 4 rounds of treatment with free or encapsulated 3M-052, the most significant increase was obtained for the 3M-052/IRIN silicasome (Figure 5C). All considered, the dual-drug silicasome was more effective than the free drug or single-drug silicasome for generating anti-PDAC immunity, which is in keeping with the notion that TLR7/8 activation is capable of boosting the IRIN-induced ICD response. We also obtained evidence that the response boosting involves LNDC participation as a key component of the cancer immunity cycle.

Noteworthy, these therapeutic outcomes were achieved without a significant change in animal body weight in any of the groups, which is in keeping with the absence of systemic toxicity (Figure S6). This notion was further confirmed by blood collection for white blood cell counting and assessment of kidney function (creatinine and urea levels), liver enzymes (ALP, AST, and ALT), blood calcium and phosphate levels, as demonstrated in Table S1. These results are also congruent with previous demonstration of improved safety of our IRIN nanocarrier, in which a supported LB is superior to a liposomal LB.[8]

Improved Pharmacokinetics of Drug delivery and Effective Silicasome Biodistribution to Orthotopic Tumors

The pharmacokinetics (PK) studies were performed in healthy B6129SF1/J mice (n=3) which received a single IV injection of free 3M-052 (2 mg/kg), free IRIN (40 mg/kg), and 3M-silicasome-IR (3M-052, 2 mg/kg; IRIN, 40 mg/kg), respectively. Plasma samples were collected at different time points over 24 h and used to measure the concentrations of 3M-052 and IRIN by HPLC. These results show that while free 3M-052 and IRIN were

rapidly cleared from the blood circulation, treatment with the dual-delivery carrier led to sustained increases in blood levels of both drugs for at least 24 h, confirming stable drug entrapment by the PEGylated LB (Figure 6).

In order to assess the particle biodistribution, a DiR-labeled dual-delivery carrier (3M-silicasome-IR-DiR) was developed for IVIS imaging, as described in the Experimental Section. The particle characteristics are shown in Figure 7A. Biodistribution was assessed in the orthotopic KPC tumor model, derived by injecting stable luciferase-transfected KPC cells into the pancreas tails of female B6129SF1/J mice, as described by us.[7] Orthotopic tumor-bearing mice (n=3–4) received a single IV injection of saline, free 3M-052 (2 mg/kg), free IRIN (40 mg/kg) and the DiR-labeled 3M-silicasome-IR (3M-052, 2 mg/kg; IRIN, 40 mg/kg), before collection of IVIS images (Figure 7B). *In vivo* IVIS imaging demonstrated effective biodistribution to the tumor site after 24 and 48 h (Figure 7C). However, since pancreas images overlap with the liver, we also performed animal sacrifice and organ explantation to collect *ex vivo* IVIS images and quantification of DiR fluorescence intensity. The right-side panel in Figure 7D shows representative images of an animal selected from each group, with the rest of the animal images on display in Figure S7. Quantitative display of DiR intensities for both animal groups demonstrated 26.5% and 23.6% label distribution to the primary tumor sites after 24 or 48 h, respectively (Figure 7D). Comparable liver biodistribution values were 37.0 % and 33.3 %, respectively, in addition to some fluorescence intensity appearing in the spleens and intestines. The spleen, similar to lymph nodes, acts as a secondary lymphoid organ in supplementing immune responses in the pancreas.

We also used the orthotopic KPC model to assess the IRIN content at the primary tumor site, using HPLC analysis. These results demonstrate that treatment with the labeled 3M-silicasome-IR carrier could increase the IRIN content at the tumor site by 36- and 49-fold, respectively, after 24 and 48 h (Figure 7E). These results agree with the improved PK data in Fig. 6. It was not possible to quantify 3M-052 levels at the tumor site because the limited threshold of HPLC analysis for this substance.

Immunotherapy efficacy of Dual-delivery Silicasomes in the Orthotopic KPC Tumor Model

While helpful to observe the chemoimmunotherapy response in subcutaneous KPC tumors, this tumor model displays a modest stromal content, differing from the extensive dysplasia seen in human PDAC. This is of relevance in considering the stromal contributions to shaping the immune-suppressive PDAC immune landscape. While genetically engineered Pdx1-cre/LSL-Kras/G12D/p53R172H) mice display many similarities to human PDAC (including the G12D KRAS mutation and TP53 loss, extensive desmoplasia, and an immune suppressive TME), the logistical constraints of animal breeding prompted as to use of an orthotopic model, instead. We have previously shown that implantation of a luciferase-expressing KPC cell line into the pancreatic tail of immunocompetent B6129SF1/J mice can be used to obtain tumor growth, with retention of human PDAC features, including a more robust stroma that resemble the heterogeneous immune landscape of the genetic animal models.[15]

Orthotopic tumor-bearing B6129SF1/J female mice were established, as described in Figure 8A. After confirming tumor growth at the pancreatic site by IVIS imaging, the tumor-bearing mice (n=5/6) received IV injection with saline, free IRIN (40 mg/kg), 3M-silicasome (3M-052, 2 mg/kg), silicasome-IR (IRIN, 40 mg/kg) and 3M-silicasome-IR (3M-052, 2 mg/kg; IRIN, 40 mg/kg) every 3 days for a total of 4 administrations (Figure 7A). Characterization of the IRIN-silicacasome (silicasome-IR or Si-IR) appear in Figure S8B. Animals continued to be monitored by i*n vivo* IVIS imaging on days 7, 15, 18, and 21, as displayed in Figure 8B. Quantitative analysis of tumor bioluminescence intensity ("region of interest") on day 21 demonstrated significant intensity decline in mice treated with the 3M-silicasome or 3M-silicasome-IR, compared to the saline control (Figure 8C). Moreover, the dual-drug silicasome had a statistically significant effect ($p < 0.05$) compared with the single-drug silicasome. These findings were further corroborated by photographs that display tumor size (Figure 8D), in addition to conducting tumor weight assessment (Figure 8E).

Following animal sacrifice on day 21, primary tumors and organs were harvested for IVIS imaging and for performing IHC analysis of the tumor immune landscape. Of note, *ex vivo* IVIS image analysis showed differences in the level of metastatic spread to the liver, kidneys, stomach, spleen, and intestines among the different treatment modalities (Figure 8F). Thus, while there was evidence for splenic involvement in the representative example displayed in Figure 8F for free IRIN, there was scant evidence of metastatic spread during treatment with single or dual drug silicasomes (Figure 8F). The comprehensive list of *ex vivo* IVIS images appears in Figure S8A.

IHC analysis was performed to assess the expression of $CD8^+$ T cells and $FoxP3^+$ Treg cells, as demonstrated in Figure 8G. This demonstrate that the dual-drug silicasome showed the highest levels of $CD8^+$ T-cell recruitment along with the largest decline in Treg cell numbers at the primary orthotopic tumor site (Figure 8G). This was also associated with the most statistically significant increase in the $CD8^+$/ Treg ratio compared to the other treatments (Figure 8G). Representative IHC images appear in Figure S9. Body weight monitoring every 2 days did not show any significant weight loss among all groups (Figure S10). There was also no evidence of toxicity elsewhere.

In this study, we demonstrate that the CD18 lipid tail of the TLR7/8 agonist, 3M-052, can be incorporated into the lipid bilayer (LB) of a mesoporous silica nanocarrier (silicasome), which can also be used for remote loading of the amphipathic chemotherapeutic agent, irinotecan. We hypothesized that co-delivery of the TLR7/8 agonist with irinotecan may be able to mount a synergistic anti-PDAC immune response, based on boosting of APC function of dendritic cells receiving an enriched supply of tumor antigens as a result of the ICD response. We demonstrated effective TLR7 activation in a HEK-Blue™ mTLR7 reporter cell line, in addition to accomplishing activation and maturation of macrophage and BMDCs. This was followed by *in vivo* experimentation, demonstrating effective generation of an anti-PDAC immune response in a subcutaneous KPC tumor model, showing evidence of enhanced tumor shrinking, increased $CD8^+$/Treg ratios and increased LNDC activation in response to the dual-delivery carrier. Moreover, further experimentation in a robust orthotopic KPC model confirmed the ability of the dual-delivery carrier to trigger a

synergistic immune response, backed by data showing improved drug delivery and tumor biodistribution. Not only do these results demonstrate the efficacy of a co-formulated drug carrier, but expand the scope of employing a chemoimmunotherapy approach for PDAC and other cancers, as recently reviewed by us.[15]

The key advance demonstrated in this communication is the impact of a co-delivered TLR7/8 agonist on a PDAC immune landscape, characterized by a paucity of neoantigens, poor antigen presentation, and interference in cytotoxic T-cell killing by a variety of immune escape or immune suppressive mechanisms. This includes dampening of the supply of conventional DC progenitors and their action as APC at the primary tumor site.[33] This is also in agreement with the poor prognosis of PDAC patients expressing a reduced number of circulatory DC, thereby necessitating therapeutic intervention to improve APC supply and DC activation at the cancer site.[34] While encapsulated irinotecan improves tumor antigen delivery to DC through its ICD effect, additional adjuvant stimuli are required for DC activation, maturation and APC function at the primary tumor as well as secondary lymphatic organ sites. It is therefore of major significance that the TLR family is widely expressed at the PDAC site and capable of improving DC function in response to danger signals. Moreover, a number of TLR agonists are available for therapeutic intervention, including synthetic imidazoquinoline agonists capable of ligating endosomal TLR7 and TLR8 receptors. This approach can be used for silicasomes and liposomes.[15]

Protected delivery of TLR7/8 agonists provides an ideal opportunity for preventing inflammatory side effects, known to include manifestations such as pyrexia, fatigue, chills, decreased lymphocyte counts, nausea, or pain at the injection site.[20] To overcome this problem localized administration of 3M-052 (MEDI-9197), either as a monotherapy or in combination with checkpoint blockade, has been attempted.[35] However, in spite of minimal systemic effects in mouse models, severe systemic effects were observed in a human phase I clinical trial, leading to abandonment of phase II trials.[20] This triggered nanocarrier development, including by absorbing 3M-052 to lipid-decorated alum oxyhydroxide nanoparticles, used as an adjuvant during tuberculosis vaccination.[36] Another approach was to encapsulate 3M-052 in PLGA nanoparticles, capable of providing even and more effective vaccination response to an HIV antigen than alum-TLR7.[28] Moreover, Wightman *et al.* showed that liposomal encapsulation of 3M-052 could also serve as a vaccine adjuvant for antibody generation against viral proteins.[25] While able to develop an in-house 3M-052 liposome (Figure S1), we prefered to develop a carrier with a more stable supported LB, as previously demonstrated for obtaining toxicity reduction for a liposomal irinotecan carrier.[8] We confirmed the safety of the silicasome carrier, showing no impact on animal weight or an impact on white blood cell counts, liver and kidney function, blood calcium, or phosphate (Table S1).

The efficacy of dual drug delivery by the 3M-silicasome-IR was demonstrated by more effective tumor shrinkage, compared to the response to the irinotecan- or 3M-silicasomes only (Figures 4B and 8C). Moreover, evidence was provided that this outcome is accomplished by immune activation, as demonstrated by the synergistic increase of $CD8^+$/Treg ratios in animals treated with the dual-delivery compared to single-drug carriers (Figures 5A and 8G). Nonetheless, the 3M-silicasome had a significant effect on its own

in the subcutaneous and orthotopic KPC tumor models (Figures 4 and 8), demonstrating the utility of the TLR7/8 pathway on its own accord for PDAC. These results are also in agreement with the findings of Michaelis *et al.*, who demonstrated effective tumor shrinkage, improved survival, and attenuation of cachexia in murine PDAC models treated with R848.[37] This outcome was also accompanied by increased $CD8^+$ T-cell infiltration and a reduction in the number of Tregs at the tumor site. Moreover, these authors used a TLR knockout model to show that the major R848 impact was on a stromal TLR7-mediated immune response, rather than an impact on cancer cells.

Importantly, our subcutaneous KPC data demonstrate the importance of TLR7 on co-stimulatory receptor (CD80 and CD86) expression on lymph node-derived $CD11c^+$ dendritic cells (Figure 5C). This agrees with the importance of lymph node participation in the cancer immunity cycle, including the irinotecan immunogenic response. Following calreticulin-mediated uptake of tumor antigens present in dying PDAC cells, participating DCs migrate to secondary lymphoid organs, where instruction of naïve T-cells allows activated, mature cytotoxic $CD8^+$ T-cells to return to the tumor site. Not only do we demonstrate that encapsulated 3M-052 delivery is capable of boosting DC activation at the site and regional lymph nodes in the subcutaneous model, but also that the DiR-labeled 3M-Si-IR biodistributes to the spleen (Figures 7C and D). This finding is commensurate with the demonstration that conjugation of a TLR7 small-molecule, 1V209, to cholesterol could be used to construct a liposome, capable of distributing to lymph nodes in CT26 colorectal cancer, 4T1 breast cancer, and Pan02 pancreatic ductal cancer models.[29] Moreover, the encapsulation of resiquimod (R848) in PLA nanoparticles was capable of regional lymph node targeting and DC uptake to enhance immunotherapy for skin cancer.[38]

In addition to impacting DC function, there are other cell types in the PDAC TME that could be impacted by TLR7 agonists. For instance, it has been shown that R848 reduces immune suppression by inducing differentiation of MDSC into macrophages and DCs.[39] The same applies to tumor-associated macrophages, including demonstration that R848 and 3M-052 are potent drivers of the M1 differentiation, including during nanoparticles delivery.[40] In addition to an expanded range of cell targets, it is appropriate to consider combining TLR7/8 with other TLR agonists, including CpG oligonucleotides, polyinosinic-polycytidylic acid, monophosphoryl 3-deacyl lipid A (3D-PHAD or 3D(6-acyl)-PHAD) for activation of TLR9, TLR3 and TLR4, respectively.[20] Moreover, several of these agonists are available as lipophilic agents for silicasome LB incorporation. This is in agreement with the demonstration that a TLR combination strategy can lead to synergistic DC activation, e.g., combining R848 with either a TLR4 agonist or a TLR3 agonist to activate multiple human DC subsets.[41] It is also possible to combine TLR7/8 agonists with other classes of immune-modulatory agents, such as the combined use with antibodies to checkpoint receptors, EGFR, HER2/neu or OX-40, as well as photothermal therapy.[20]

In addition to chemotherapy-induced immunogenic cell death, there are also radiation or other physical stimuli that can be used to induce ICD (also referred to as and abscopal effect). This includes therapeutic modalities such as radiotherapy (RT), photothermal therapy (PTT), and photodynamic therapy (PDT), which are all currently used for boosting immunotherapy.[42] RT has been shown to induce the expression of CRT, HMGB1 and HSP

70 on the surface of dying tumor cells towards accomplishing an abscopal therapeutic effect.[43,44] PTT is capable of killing tumor cells through a hyperthermia response that leads to DNA damage, protein denaturation, and disruption of the cellular membrane. This allows the release of tumor antigens, heat shock proteins, and pro-inflammatory cytokines that promote immune activation.[45] In contrast, the impact of PDT involves damage to the tumor cells by the generation of highly reactive oxygen species including superoxide anion, hydroperoxide radicals, and hydroxyl radicals.[46] These oxidative stress stimuli induce tumor cell death in combination with cell stress responses that provide danger signals to the immune system. Since a number of nanocarriers have been developed for generating RT, PTT, and PDT-mediated immune responses, it is theoretically possible to combine the delivery of TLR7/8 agonists with these carriers. For instance, liposomes could be designed to allow a lipophilic agent such as 3M-052 loaded into the lipid bilayer of carrier that also include self-assembled photothermal gold nanoparticles or a photothermal dye (Figure S1).

Conclusions

In summary, we developed a synergistic drug carrier to co-deliver a chemotherapeutic agent with a TLR7/8 agonist for augmenting the ICD-inducing effect of irinotecan by the DC activating effect of 3M-052, including at participating lymph nodes. Based on the fact that we have already achieved upscale manufacturing of a single drug silicasome platform, these results hold great promise for strengthening this platform for use in the treatment of PDAC and other cancers. Where necessary, combination therapy can also be achieved by synthesizing liposomes that combine irinotecan and 3M-052. Moreover, it is also possible to load other ICD-inducing chemotherapeutic agents (e.g., doxorubicin, mitoxantrone, oxaliplatin) into these carriers, where the chemoimmunotherapy effects can be combined with co-delivered TLR agonists, small-molecule PD1 inhibitors, GSK3 inhibitors and TGF-beta inhibitors to intervene in multiple cancer types.

Methods

Materials

1,2-distearoyl-sn-glycero-3-phosphocholine (DSPC), cholesterol (Chol) and 1,2-distearoyl-sn-glycero-3-phosphoethanolamine-N-[methoxy(polyethylene glycol)-2000] (ammonium salt) (DSPE-PEG2000) were purchased from Avanti Polar Lipids, USA. Fetal bovine serum (FBS) was purchased from Gemini Bio Products. Dulbecco's modified Eagle medium (DMEM), Roswell Park Memorial Institute (RPMI) 1640 medium, penicillin, streptomycin, DiD' solid (DiIC$_{18}$(5) solid (1,1′-Dioctadecyl-3,3,3′,3′-Tetramethylindodicarbocyanine, 4-Chlorobenzenesulfonate Salt)) and DiR' (DiIC$_{18}$(7) (1,1′-Dioctadecyl-3,3,3′,3′-Tetramethylindotricarbocyanine Iodide)) were purchased from Invitrogen. 3M-052 (a.k.a. Telratolimod) and Cell Counting Kit-8 (CCK-8) were purchased from MedChemExpress, USA. Irinotecan hydrochloride trihydrate was purchased from LC Laboratories, USA. ACK Lysing Buffer was purchased from Thermo Fisher Scientific Inc., USA. HEPES (4-(2-hydroxyethyl)-1-piperazineethanesulfonic acid), dextrose, DNase I, and Collagenases (Type II and IV) were purchased from Sigma-Aldrich, USA. Recombinant Murine granulocyte-macrophage colony-stimulating factor (GM-CSF) was purchased from

PeproTech, USA. ELISA kits for quantitative measurement of murine IL-12/IL-23 p40 and TNF-alpha levels were purchased from R&D Systems, Inc., USA. The murine assay for assessing TLR-induced reporter gene activity in HEK 293 cells (HEK-Blue™ Detection) as well as R848 (Resiquimod) were purchased from InvivoGen, USA. Anti-mouse CD16/32 antibody, Zombie Violet™, Cell Staining Buffer, FITC anti-mouse CD11c antibody, anti-mouse CD80 antibody, PerCP/Cyanine5.5 anti-mouse CD45.2 antibody, anti-mouse CD11c antibody, PE anti-mouse CD80 antibody, and FITC anti-mouse CD86 antibody were purchased from BioLegend, USA.

Synthesis, Purification, and Characterization of 3M-silicasome-IR

Bare MSNPs were synthesized and purified by extensive acidic ethanol washing to remove the CTAC detergent, previously described by us.[8] The trapping agent, TEA_8SOS, was prepared from a commercially available sucrose octasulfate (SOS) sodium salt through an ion-exchange chromatography procedure, previously described by us.[7] This was followed by particle coating with a lipid bilayer, which serves three purposes: (i) providing a stable encapsulating bilayer that protects drug leakage as previously described by us;[7] (ii) facilitating remote loading of irinotecan through the bilayer, with assistance of the protonating agent in the porous interior; (iii) using the bilayer for inclusion of a second lipophilic drug, 3M-052. The success of the alcohol-exchange coating strategy can be attributed to the rapid aggregation of the lipid components onto the MSNP surface, assisted by strong van der Waals and electrostatic interactions, which are responsible for rapidly encapsulation of the entire surface area in a bilayer with reduced lipid flux and high stability.[8] For the synthesis of the 3M-silicasome, a mixture of 50 mg of 3M-052 and lipids (DSPC/Chol/DSPE-PEG2000/3M-052, in the molar ratio of 55.5:38.5:2.7:3.3) was dissolved in 0.1 mL pure ethanol at 65 °C. Then, 1 mL of a preheated (65 °C) solution, containing 40 mg MSNP soaked in 80 mM TEA_8SOS trapping agent, was poured into the lipid solution and mixed with a pipette. This mixture was treated by probe sonication with a 15/15 s on/off working cycle and a power output of 32.5 W. After 15 min, the sample was purified by size-exclusion chromatography, using a Sepharose CL-4B column with a HEPES (5 mM HEPES, 5% dextrose, pH 6.5) buffer elution to remove the free trapping agent.

For IRIN remote loading, 20 mg irinotecan was dissolved in 2 mL HEPES-buffered dextrose, before mixing and incubation of the TEA_8SOS-loaded 3M-silicasome at 65 °C for 30 min. The reaction was quenched on ice water for another 30 min, following which the irinotecan-loaded silicasome, designated 3M-silicasome-IR, was washed three times by centrifugation at 15 000 rpm for 30 min in a HEPES-buffered NaCl solution (4.05 mg/mL HEPES, 8.42 mg/mL NaCl, pH 7.2). In addition to the synthesis of dual-delivery particles, we also constructed particles capable of delivering IRIN only by eliminating 3M from the lipid suspension.

In experiments requiring particles for the performance of *in vitro* and *in vivo* imaging, DiD and DiR labeling was performed by adding 0.2 mg DiD or DiR into the mixture of 50 mg of 3M-052 and lipids (DSPC/Chol/DSPE-PEG2000/3M-052, in the molar ratio of 55.5:38.5:2.7:3.3). The procedure used for DiD-3M-silicasome or DiR-3M-silicasome-IR was the same as that of 3M-silicasome-IR.

For the characterization of the nanocarriers, loading capacity was determined by calculating the weight ratio of 3M-052 or IRIN relative to the total particle composition. MSNP mass was determined by TGA. The concentrations of 3M-052 and IRIN were determined by the UV-vis absorbance at 320 nm and 360 nm respectively (M5e, Molecular Device, USA). Particle hydrodynamic size, size distribution, and zeta potential were measured by a ZETAPALS instrument (Brookhaven Instruments Corporation). The uniformity and integrity of the lipid-coated particles containing 3M-052, with or without IRI remote loading, were characterized by the performance of cryoEM, using a TF20 FEI Tecnai-G2 instrument.

Cell Culture

KRAS transformed murine pancreatic adenocarcinoma (KPC) cells, derived from a spontaneous tumor originating in a transgenic KrasLSL-G12D/+; Trp53LSL-R172H/+; Pdx-1-Cre mouse model, was used for stable transfection with a luciferase-based lentiviral vector to derive KPC-luc cells. The cells as well as the murine macrophage-like cell line (RAW264.7) cells were cultured in DMEM with 10% (v/v) FBS, 100 units/mL of penicillin, and 100 mg/mL of streptomycin under 37 °C with 5% CO_2.

Bone marrow-derived dendritic cells (BMDCs) were prepared according to our established procedure, with a slight modification.[47] Bone marrow cells flushed from the femur and tibia of B6/129 mice were collected and red blood cells were lysed by incubating in ACK Lysing Buffer. On the 1st day, cells were cultured in a 24-well plate with 1 mL/well of RPMI-1640 medium supplemented with 10% (v/v) FBS, 100 units/mL of penicillin, 100 mg/mL of streptomycin and 20 ng/mL GM-CSF under 37 °C with 5% CO_2. On the 3rd and 5th day, the culture medium was replaced to include GM-CSF for an additional 2 days. Immature BMDCs were acquired by using non-adherent or loosely adherent cells for centrifugation at 1400 rpm for 5 min.

Commercially acquired HEK-Blue™ mTLR7 cells, derived from the human embryonic kidney HEK293 cell line, were used to confirm the generation of TLR7 signaling by free and encapsulated 3M-052, demonstrating NF-κB/AP1-induced activation of the transgene promotor leads to release of secreted embryonic alkaline phosphatase (SEAP). These cells were cultured in DMEM medium supplemented with 10% (v/v) FBS, 100 units/mL of penicillin, 100 mg/mL of streptomycin, and 10 μg/ml of Blasticidin, and 100 μg/ml of Zeocin.

Cellular response of TLR7 reporter cell line

A suspension of 2.2×10^5 cells/mL was prepared in HEK-Blue™ Detection medium, following which 180 μL aliquots (around 4×10^4 cells/well) were dispensed into the wells of a 96-well plate. This was followed by the addition of 20 μL PBS (negative control), R848 (positive control), free 3M-052, and 3M-silicasome to achieve a concentration range of 0.01 to 10 μM. Cells were incubated at 37 °C in 5% CO_2 for 20 h. The release of SEAP into the supernatant was determined, using a microplate reader at 630 nm.

Assessment of RAW264.7 and BMDC responses to TLR7 activation

RAW264.7 cells (1×10^5 cells/well) were cultured in 48-well plates for 24 h, before the addition of PBS or 10 μM concentrations of R848, free 3M-052 or the 3M-silicasome for a further 21 h. Immature BMDCs (5×10^5 cells/well) were cultured in 24-well plates, receiving the same dose of R848, free 3M-052, and 3M-silicasome for 21 h. The cellular suspensions from each well were collected and centrifuged to obtain supernatants for ELISA analysis. This included measurement of murine IL-12p40 and TNF-α levels, using each vendor's protocol.

For flow cytometry analysis of surface markers, cells were washed with cell staining buffer, before staining RAW264.7 cells with anti-CD80 or BMDCs with FITC-conjugated anti-CD11c and anti--CD80 on ice, according to the manufacturer's instructions. The assessment of the differentiation and activation markers were evaluated by flow cytometry (LSRFortessa; BD Biosciences), analyzed by FlowJo software.

Cell viability test, cellular uptake and in vitro killing effects

For cell viability testing, KPC and RAW264.7 cells were seeded in 100 μL culture medium in 96-well plates at a density of $3–5 \times 10^3$ cells per well for 24 h, before the addition of 100 μL fresh medium containing the 3M-silicasome at 3M-052 concentrations of 2, 4, 8, 16, 20, 30, 40 μM for a further 48 h. After removal, MTS was added in fresh medium at a concentration of 317 μg/mL for an additional 1 to 2 h, before the determination of UV-visible absorption at 490 nm in a microplate reader. Cell viability (%) was calculated using the formula: $(OD_{sample} - OD_{blank})/(OD_{control} - OD_{blank}) \times 100$.

To assess cellular nanocarrier uptake, the DiD-3M-silicasome was incubated with RAW264.7 cells (1×10^5 cells/well) to deliver concentrations of 2, 5, and 10 μM for 21 h. The same procedure was followed for immature BMDCs (5×10^5 cells/well), incubated with the same concentration range of the DiD-3M-silicasome for 21 h in a 24-well plate. The cells were harvested and washed before assessing DiD fluorescence in a flow cytometer, using FlowJo software.

To verify KPC cytotoxicity, cells seeded in 96-well plates were incubated with different concentrations (50, 100, 200, 300, 400, and 500 μM) of free IRIN and the 3M-silicasome-IR for 48 h. 20 μL of CCK-8 solution was added to each well and the plates were incubated for an additional 1–2 h in an incubator. The absorbance of each well was assessed at 450 nm in a microplate reader. Cytotoxicity (% dead cells) was calculated using the formula: $(OD_{sample} - OD_{blank})/(OD_{control} - OD_{blank}) \times 100$.

Assessment of 3M-052 and IRIN pharmacokinetics

All animal experimental protocols were approved by the UCLA Animal Research Committee. The PK study was carried out in 8–10-week-old healthy female B6129SF1/J mice which received one IV injection of free 3M-052, free IRIN, and 3M-silicasome-IR at dose equivalents of 2 mg/kg and 40 mg/kg for 3M-052 and IRIN, respectively. Blood collections were performed at 1, 5, 24, and 48 h post-injection, and the plasma was collected by centrifuging at 3500 rpm in plasma collecting tubes. Free 3M-052 and IRIN were

extracted by methanol and measured by HPLC. The details are described in the HPLC analysis section.

Assessment of carrier efficacy, using a subcutaneous KPC tumor model

A subcutaneous KPC tumor model was established in immunocompetent B6129SF1/J mice, using protocols approved by the UCLA Animal Research Committee. Briefly, 100 μL of a DMEM/Matrigel (1:1 v/v) suspension, containing 1×10^6 KPC cells, was subcutaneously injected into the right flank of female B6129SF1/J mice, 8–10 weeks old. Tumor-bearing mice were randomly assigned into 5 groups (n = 6–7), which received IV injections of saline, free 3M-052, free IRIN, 3M-silicasome, and 3M-silicasome-IR, respectively, when tumor sizes reached ~100 mm^3. Injections were given every 3–4 days, using the dosing schedule that delivers the equivalent of 2 mg/kg and 40 mg/kg, respectively, for 3M-052 and IRIN. Subcutaneous KPC tumor size and animal weight were monitored every 2 days. The tumor size was calculated according to the formula: $(Width^2 \times Length)/2$.

Following animal sacrifice, photographs were obtained of the harvested tumors, which were subsequently fixed in 10% formalin for IHC staining by the UCLA Translational Pathology Core Laboratory. Image processing was performed using Aperio ImageScope software (Leica). IHC analysis was performed to assess tumor staining intensity for CD8 and FoxP3. Additionally, we assessed the immune response in the draining inguinal lymph nodes (LNs) harvested from the sacrificed animals. The lymph nodes were washed in PBS, before slicing into small fragments. These fragments were placed into a 6-well plate, incubated in 5 mL digestion medium (1 mg/mL collagenase, type II, 1 mg/mL collagenase, type IV and 0.2 mg/mL DNase, Type I) at 37°C for 2–3 h. Single-cell suspensions were obtained by passing the tissue digests through a 70 mm cell strainer, followed by washing in a cell staining buffer. For the performance of flow cytometry analysis, cells were stained on ice with PerCP/Cyanine5.5-CD45 and anti-CD11c antibodies to analyze the number of activated DCs, in addition to the use of PE-CD80 and FITC-CD86 antibodies to assess DC maturation. The flow cytometry procedure for the analysis of these phenotypes, with the use of FlowJo software, is explained in Figure S5.

We also collected blood for separating serum after centrifugation at 3500 rpm for 20 min. The following biochemical parameters were assayed by UCLA Division of Laboratory Animal Medicine (DLAM) diagnostic laboratory services: white blood cell (WBC), alkaline phosphatase (ALP), aspartate aminotransferase (AST), alanine aminotransferase (ALT), blood urea nitrogen (BUN), creatinine, calcium, and phosphorus.

Assessment of nanocarrier and drug biodistribution in an orthotopic KPC-luc tumor model

A DiR-labeled 3M-silicasome-IR nanocarrier was prepared for biodistribution assessment in a KPC-derived orthotopic tumor model in immunocompetent B6129SF1/J mice, as previously described by us.[7] The animal protocol received institutional approval. Briefly, a 50 μL suspension of DMEM/Matrigel (6:4 v/v), containing 8×10^5 KPC-luc cells, was injected into the pancreas tail of female B6129SF1/J mice, using a limited surgical procedure under anesthesia. After 15 days, tumor-bearing mice were randomly assigned into 5 treatment groups (n = 3–4), designed to receive one IV injection of saline, free

IRIN, and DiR-3M-silicasome-IR. The dose equivalent for IRIN was 40 mg/kg. The *in vivo* fluorescence intensity of the DiR label group was performed in a Xenogen IVIS imaging system 24 and 48 h after IV injection. Following animal sacrifice, tumors and major organs were harvested from the DiR-3M-silicasome-IR treated group, and also used for *ex vivo* IVIS imaging and quantitative analysis. In addition, tumors were also collected from all groups to determine IRIN contents by HPLC analysis.

Assessment of the therapeutic efficacy in the orthotopic KPC-luc tumor model

50 μL of a DMEM/Matrigel (6:4 v/v) suspension, containing 8×10^5 KPC-luc cells, was injected into the tail of the pancreas in female B6129SF1/J mice by a survival surgery procedure. One week after the surgery, IVIS imaging was used to confirm the establishment of bioluminescent tumors, following which animals were randomly assigned into 5 treatment groups (n = 5), earmarked for IV injection of saline, free IRIN, 3M-silicasome, silicasome-IR, and 3M-silicasome-IR, respectively, every 3 days. The dose equivalents of 3M-052 and IRIN were 2 mg/kg and 40 mg/kg per dose, respectively. Animal weight was monitored every 2 days.

To perform the bioluminescence imaging of the luciferase-expressing tumors, mice were injected intraperitoneal with 50 mg/kg D-Luciferin on day 7, 15, 18, and 21. *Ex vivo* IVIS images of tumors and major organs, collected from sacrificed animals, were obtained on day 21. In addition, we also obtained photographs and weighed the harvested tumors, which were subsequently fixed in 10% formalin for the performance of IHC staining. IHC analysis was the same as described above.

HPLC Analysis

The harvested tumor and organ samples, collected in the drug biodistribution experiment, were weighed and homogenized. The collected plasma, tumor, and organ homogenates were extracted in methanol, using 1:5, 1:4, and 1:3 v/v dilutions, respectively. The extracts were vortexed for 20 s and centrifuged at 13000 rpm for 10 min, following which the drug-containing supernatants were filtrated through 0.22 μm filters to perform HPLC analysis. The HPLC system is operated by a Knauer Smartline Pneumatic Pump, C18 column, K-2600 spectrophotometer, and Gina data acquisition software. The mobile phase consisted of mobile phase A (0.01% trifluoroacetic acid in water) and mobile phase B (0.01% trifluoroacetic acid in methanol) as 70% A and 30% B (v/v). A 20 μL of the sample was injected to measure the 3M-052 and IRIN absorptions at 320 and 360 nm. The 3M-052 and IRIN standard curves were generated over the maximal concentrations of 40 and 100 μg/mL respectively.

Statistical Analysis

Differences among groups were estimated by one-way ANOVA analysis. Data were expressed as mean ± standard deviation (S.D.), representing at least three independent experiments. A statistically significant difference was considered at $^{*}p < 0.05$; $^{**}p < 0.01$; $^{***}p < 0.001$; $^{\#}p < 0.05$; $^{\#\#}p < 0.01$ and $^{\#\#\#}p < 0.001$, as indicated in the figure legends.

Supplementary Material

Refer to Web version on PubMed Central for supplementary material.

ACKNOWLEDGMENTS

This study was supported by the U.S. Public Health Service Grant, R01CA247666-03. We also acknowledge the use of the Preclinical Imaging Technology Center, the Translational Pathology Core Laboratory (TPCL), the Electron Imaging Center for Nanomachines (EICN), the Molecular Instrumentation Center, and the CNSI Advanced Light Microscopy/Spectroscopy (ALMS) Shared Facility at UCLA.

References

(1). Siegel RL; Miller KD; Fuchs HE; Jemal A Cancer Statistics, 2021. CA-Cancer J. Clin 2021, 71, 7–33. [PubMed: 33433946]

(2). Siegel RL; Miller KD; Fuchs HE; Jemal A Cancer Statistics, 2022. CA-Cancer J. Clin 2022, 72, 7–33. [PubMed: 35020204]

(3). Chu GC; Kimmelman AC; Hezel AF; DePinho RA Stromal Biology of Pancreatic Cancer. J. Cell. Biochem 2007, 101, 887–907. [PubMed: 17266048]

(4). Wang-Gillam A; Li C-P; Bodoky G; Dean A; Shan Y-S; Jameson G; Macarulla T; Lee K-H; Cunningham D; Blanc JF; Hubner RA; Chiu C-F; Schwartsmann G; Siveke JT; Braiteh F; Moyo V; Belanger B; Dhindsa N; Bayever E; Von Hoff DD; et al. Nanoliposomal Irinotecan with Fluorouracil and Folinic Acid in Metastatic Pancreatic Cancer after Previous Gemcitabine-Based Therapy (NAPOLI-1): A Global, Randomised, Open-Label, Phase 3 Trial. The Lancet 2016, 387, 545–557.

(5). Frampton JE Liposomal Irinotecan: A Review in Metastatic Pancreatic Adenocarcinoma. Drugs 2020, 80, 1007–1018. [PubMed: 32557396]

(6). Meng H; Wang M; Liu H; Liu X; Situ A; Wu B; Ji Z; Chang CH; Nel AE Use of a Lipid-Coated Mesoporous Silica Nanoparticle Platform for Synergistic Gemcitabine and Paclitaxel Delivery to Human Pancreatic Cancer in Mice. ACS Nano 2015, 9, 3540–3557. [PubMed: 25776964]

(7). Liu X; Situ A; Kang Y; Villabroza KR; Liao Y; Chang CH; Donahue T; Nel AE; Meng H Irinotecan Delivery by Lipid-Coated Mesoporous Silica Nanoparticles Shows Improved Efficacy and Safety over Liposomes for Pancreatic Cancer. ACS Nano 2016, 10, 2702–2715. [PubMed: 26835979]

(8). Liu X; Jiang J; Chan R; Ji Y; Lu J; Liao Y-P; Okene M; Lin J; Lin P; Chang CH; Wang X; Tang I; Zheng E; Qiu W; Wainberg ZA; Nel AE; Meng H Improved Efficacy and Reduced Toxicity Using a Custom-Designed Irinotecan-Delivering Silicasome for Orthotopic Colon Cancer. ACS Nano 2019, 13, 38–53. [PubMed: 30525443]

(9). Liu X; Jiang J; Liao Y-P; Tang I; Zheng E; Qiu W; Lin M; Wang X; Ji Y; Mei K-C; Liu Q; Chang CH; Wainberg ZA; Nel AE; Meng H Combination Chemo-Immunotherapy for Pancreatic Cancer Using the Immunogenic Effects of an Irinotecan Silicasome Nanocarrier Plus Anti-PD-1. Adv. Sci 2021, 8, 2002147.

(10). Kepp O; Menger L; Vacchelli E; Locher C; Adjemian S; Yamazaki T; Martins I; Sukkurwala AQ; Michaud M; Senovilla L; Galluzzi L; Kroemer G; Zitvogel L Crosstalk between ER Stress and Immunogenic Cell Death. Cytokine Growth Factor Rev. 2013, 24, 311–318. [PubMed: 23787159]

(11). Bezu L; Gomes-da-Silva LC; Dewitte H; Breckpot K; Fucikova J; Spisek R; Galluzzi L; Kepp O; Kroemer G Combinatorial Strategies for the Induction of Immunogenic Cell Death. Front. Immunol 2015, 6,1664–3224.

(12). Kroemer G; Galluzzi L; Kepp O; Zitvogel L Immunogenic Cell Death in Cancer Therapy. Annu. Rev. Immunol 2013, 31, 51–72. [PubMed: 23157435]

(13). Galluzzi L; Buqué A; Kepp O; Zitvogel L; Kroemer G Immunogenic Cell Death in Cancer and Infectious Disease. Nat. Rev. Immunol 2017, 17, 97–111. [PubMed: 27748397]

(14). Chen DS; Mellman I Oncology Meets Immunology: The Cancer-Immunity Cycle. Immunity 2013, 39, 1–10. [PubMed: 23890059]

(15). Nel AE; Mei K-C; Liao Y-P; Liu X Multifunctional Lipid Bilayer Nanocarriers for Cancer Immunotherapy in Heterogeneous Tumor Microenvironments, Combining Immunogenic Cell Death Stimuli with Immune Modulatory Drugs. ACS Nano 2022, 16, 5184–5232. [PubMed: 35348320]

(16). Akira S; Takeda K; Kaisho T Toll-like Receptors: Critical Proteins Linking Innate and Acquired Immunity. Nat. Immunol 2001, 2, 675–680. [PubMed: 11477402]

(17). Takeuchi O; Akira S Pattern Recognition Receptors and Inflammation. Cell 2010, 140, 805–820. [PubMed: 20303872]

(18). Takeda K; Akira S Toll-like Receptors in Innate Immunity. Int. Immunol 2005, 17, 1–14. [PubMed: 15585605]

(19). Leulier F; Lemaitre B Toll-like Receptors — Taking an Evolutionary Approach. Nat. Rev. Genet 2008, 9, 165–178. [PubMed: 18227810]

(20). Bhagchandani S; Johnson JA; Irvine DJ Evolution of Toll-like Receptor 7/8 Agonist Therapeutics and Their Delivery Approaches: From Antiviral Formulations to Vaccine Adjuvants. Adv. Drug Deliv.Rev 2021, 175, 113803. [PubMed: 34058283]

(21). Iwasaki A; Medzhitov R Toll-like Receptor Control of the Adaptive Immune Responses. Nat. Immunol 2004, 5, 987–995. [PubMed: 15454922]

(22). Ryu J; Yang FC A Review of Topical Imiquimod in the Management of Basal Cell Carcinoma, Actinic Keratoses, and Other Skin Lesions. Clin. Med. Ther 2009, 1, 1557–1575.

(23). Hengge U; Benninghoff B; Ruzicka T; Goos M Topical Immunomodulators—Progress towards Treating Inflammation, Infection, and Cancer. Lancet Infect. Dis 2001, 1, 189–198. [PubMed: 11871495]

(24). Engel AL; Holt GE; Lu H The Pharmacokinetics of Toll-like Receptor Agonists and the Impact on the Immune System. Expert Rev. Clin. Pharmacol 2011, 4, 275–289. [PubMed: 21643519]

(25). Smirnov D; Schmidt JJ; Capecchi JT; Wightman PD Vaccine Adjuvant Activity of 3M-052: An Imidazoquinoline Designed for Local Activity without Systemic Cytokine Induction. Vaccine 2011, 29, 5434–5442. [PubMed: 21641953]

(26). Wang Q; Barry MA; Seid CA; Hudspeth EM; McAtee CP; Heffernan MJ 3M-052 as an Adjuvant for a PLGA Microparticle-Based Leishmania Donovani Recombinant Protein Vaccine. J. Biomed. Mater. Res. - B Appl. Biomater 2018, 106, 1587–1594. [PubMed: 28804955]

(27). Auderset F; Belnoue E; Mastelic-Gavillet B; Lambert P-H; Siegrist C-A A TLR7/8 Agonist-Including DOEPC-Based Cationic Liposome Formulation Mediates Its Adjuvanticity Through the Sustained Recruitment of Highly Activated Monocytes in a Type I IFN-Independent but NF-KB-Dependent Manner. Front. Immunol 2020, 11, 1664–3224. [PubMed: 32754161]

(28). Kasturi SP; Rasheed MAU; Havenar-Daughton C; Pham M; Legere T; Sher ZJ; Kovalenkov Y; Gumber S; Huang JY; Gottardo R; Fulp W; Sato A; Sawant S; Stanfield-Oakley S; Yates N; LaBranche C; Alam SM; Tomaras G; Ferrari G; Montefiori D; Wrammert J; et al. 3M-052, a Synthetic TLR-7/8 Agonist, Induces Durable HIV-1 Envelope–Specific Plasma Cells and Humoral Immunity in Nonhuman Primates. Sci. Immunol 2020, 5, eabb1025. [PubMed: 32561559]

(29). Wan D; Que H; Chen L; Lan T; Hong W; He C; Yang J; Wei Y; Wei X Lymph-Node-Targeted Cholesterolized TLR7 Agonist Liposomes Provoke a Safe and Durable Antitumor Response. Nano Lett. 2021, 21, 7960–7969. [PubMed: 34533963]

(30). Hiraoka N; Onozato K; Kosuge T; Hirohashi S Prevalence of FOXP3+ Regulatory T Cells Increases During the Progression of Pancreatic Ductal Adenocarcinoma and Its Premalignant Lesions. Clin. Cancer Res 2006, 12, 5423–5434. [PubMed: 17000676]

(31). Wartenberg M; Zlobec I; Perren A; Koelzer VH; Gloor B; Lugli A; Eva K Accumulation of FOXP3+T-Cells in the Tumor Microenvironment Is Associated with an Epithelial-Mesenchymal-Transition-Type Tumor Budding Phenotype and Is an Independent Prognostic Factor in Surgically Resected Pancreatic Ductal Adenocarcinoma. Oncotarget 2015, 6, 4190–4201. [PubMed: 25669968]

(32). Saleh R; Elkord E FoxP3+ T Regulatory Cells in Cancer: Prognostic Biomarkers and Therapeutic Targets. Cancer Lett. 2020, 490, 174–185. [PubMed: 32721551]

(33). Hegde S; Krisnawan VE; Herzog BH; Zuo C; Breden MA; Knolhoff BL; Hogg GD; Tang JP; Baer JM; Mpoy C; Lee KB; Alexander KA; Rogers BE; Murphy KM; Hawkins WG; Fields RC; DeSelm CJ; Schwarz JK; DeNardo DG Dendritic Cell Paucity Leads to Dysfunctional Immune Surveillance in Pancreatic Cancer. Cancer Cell 2020, 37, 289–307.e9. [PubMed: 32183949]

(34). Meyer MA; Baer JM; Knolhoff BL; Nywening TM; Panni RZ; Su X; Weilbaecher KN; Hawkins WG; Ma C; Fields RC; Linehan DC; Challen GA; Faccio R; Aft RL; DeNardo DG Breast and Pancreatic Cancer Interrupt IRF8-Dependent Dendritic Cell Development to Overcome Immune Surveillance. Nat. Commun 2018, 9, 1250. [PubMed: 29593283]

(35). Mullins SR; Vasilakos JP; Deschler K; Grigsby I; Gillis P; John J; Elder MJ; Swales J; Timosenko E; Cooper Z; Dovedi SJ; Leishman AJ; Luheshi N; Elvecrog J; Tilahun A; Goodwin R; Herbst R; Tomai MA; Wilkinson RW Intratumoral Immunotherapy with TLR7/8 Agonist MEDI9197 Modulates the Tumor Microenvironment Leading to Enhanced Activity When Combined with Other Immunotherapies. J. Immunother. Cancer 2019, 7, 244. [PubMed: 31511088]

(36). Fox CB; Orr MT; Van Hoeven N; Parker SC; Mikasa TJT; Phan T; Beebe EA; Nana GI; Joshi SW; Tomai MA; Elvecrog J; Fouts TR; Reed SG Adsorption of a Synthetic TLR7/8 Ligand to Aluminum Oxyhydroxide for Enhanced Vaccine Adjuvant Activity: A Formulation Approach. J. Control. Release 2016, 244, 98–107. [PubMed: 27847326]

(37). Michaelis KA; Norgard MA; Zhu X; Levasseur PR; Sivagnanam S; Liudahl SM; Burfeind KG; Olson B; Pelz KR; Angeles Ramos DM; Maurer HC; Olive KP; Coussens LM; Morgan TK; Marks DL The TLR7/8 Agonist R848 Remodels Tumor and Host Responses to Promote Survival in Pancreatic Cancer. Nat. Commun 2019, 10, 4682. [PubMed: 31615993]

(38). Widmer J; Thauvin C; Mottas I; Nguyen VN; Delie F; Allémann E; Bourquin C Polymer-Based Nanoparticles Loaded with a TLR7 Ligand to Target the Lymph Node for Immunostimulation. Int. J. Pharm 2018, 535, 444–451. [PubMed: 29157965]

(39). Lee M; Park C-S; Lee Y-R; Im S-A; Song S; Lee C-K Resiquimod, a TLR7/8 Agonist, Promotes Differentiation of Myeloid-Derived Suppressor Cells into Macrophages and Dendritic Cells. Arch. Pharm. Res 2014, 37, 1234–1240. [PubMed: 24748512]

(40). Rodell CB; Arlauckas SP; Cuccarese MF; Garris CS; Li R; Ahmed MS; Kohler RH; Pittet MJ; Weissleder R TLR7/8-Agonist-Loaded Nanoparticles Promote the Polarization of Tumour-Associated Macrophages to Enhance Cancer Immunotherapy. Nat. Biomed. Eng 2018, 2, 578–588. [PubMed: 31015631]

(41). Napolitani G; Rinaldi A; Bertoni F; Sallusto F; Lanzavecchia A Selected Toll-like Receptor Agonist Combinations Synergistically Trigger a T Helper Type 1–Polarizing Program in Dendritic Cells. Nat. Immunol 2005, 6, 769–776. [PubMed: 15995707]

(42). Li Z; Lai X; Fu S; Ren L; Cai H; Zhang H; Gu Z; Ma X; Luo K Immunogenic Cell Death Activates the Tumor Immune Microenvironment to Boost the Immunotherapy Efficiency. Adv. Sci 2022, 2201734.

(43). Apetoh L; Ghiringhelli F; Tesniere A; Obeid M; Ortiz C; Criollo A; Mignot G; Maiuri MC; Ullrich E; Saulnier P; Yang H; Amigorena S; Ryffel B; Barrat FJ; Saftig P; Levi F; Lidereau R; Nogues C; Mira J-P; Chompret A; Joulin V; Clavel-Chapelon F; Bourhis J; André F; Delaloge S; Tursz T; Kroemer G; Zitvogel L Toll-like Receptor 4–Dependent Contribution of the Immune System to Anticancer Chemotherapy and Radiotherapy. Nat. Med 2007, 13 (9), 1050–1059. [PubMed: 17704786]

(44). Ngwa W; Irabor OC; Schoenfeld JD; Hesser J; Demaria S; Formenti SC Using Immunotherapy to Boost the Abscopal Effect. Nat. Rev. Cancer 2018, 18 (5), 313–322. [PubMed: 29449659]

(45). Ma Y; Zhang Y; Li X; Zhao Y; Li M; Jiang W; Tang X; Dou J; Lu L; Wang F; Wang Y Near-Infrared II Phototherapy Induces Deep Tissue Immunogenic Cell Death and Potentiates Cancer Immunotherapy. ACS Nano 2019, 13 (10), 11967–11980. [PubMed: 31553168]

(46). Alzeibak R; Mishchenko TA; Shilyagina NY; Balalaeva IV; Vedunova MV; Krysko DV Targeting Immunogenic Cancer Cell Death by Photodynamic Therapy: Past, Present and Future. J. Immunother. Cancer 2021, 9 (1), e001926. [PubMed: 33431631]

(47). Inaba K; Inaba M; Romani N; Aya H; Deguchi M; Ikehara S; Muramatsu S; Steinman RM Generation of Large Numbers of Dendritic Cells from Mouse Bone Marrow Cultures Supplemented with Granulocyte/Macrophage Colony-Stimulating Factor. J. Exp. Med 1992, 176, 1693–1702. [PubMed: 1460426]

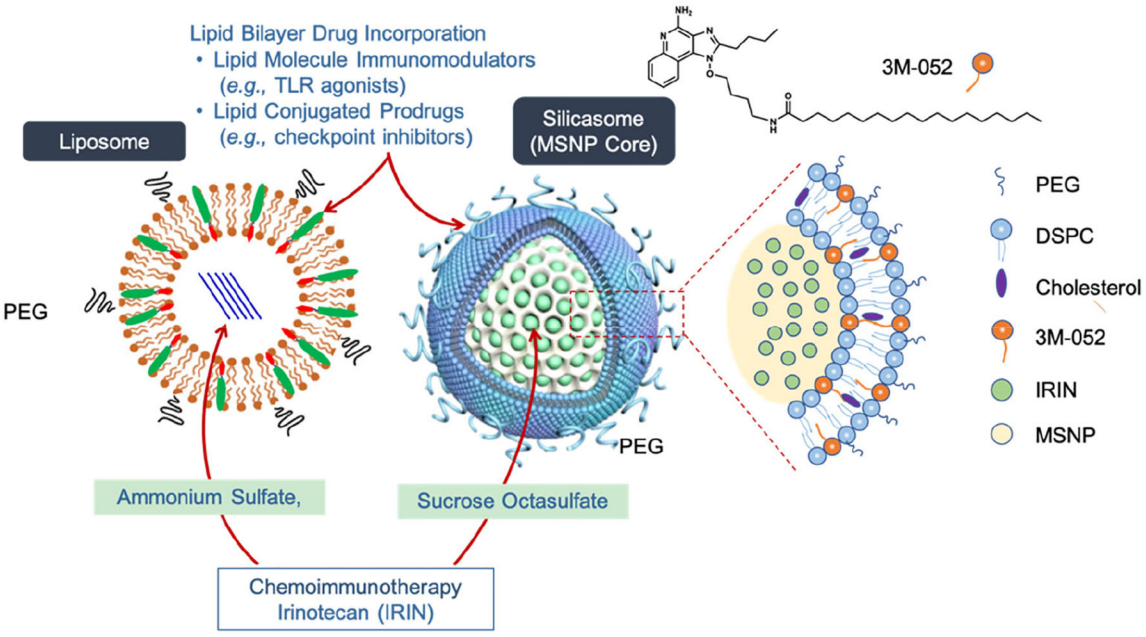

Figure 1. Schematic explaining the key design features for co-formulated drug delivery by lipid bilayer coated silicasomes and liposomes.

The basic approach to drug coformulation is to use the hydrophilic interior of these carriers for remote loading of amphiphilic drugs, such as irinotecan, while employing the lipophilic bilayer to incorporate synthetic lipid moieties and prodrugs. The lipid moieties include synthetic agents with immune stimulatory activity, such as 3M-052 (a.k.a. Telratolimod). 3M-052 contains a C18 lipid tail that facilitates bilayer incorporation, which tested in a liposome to obtain optimal LB composition before applying that to the design of the MSNP bilayer. The schematic also shows that, in addition to 3M-052, the LB can be used, to incorporate a list of lipid-conjugated prodrugs that can provide immune checkpoint blockade or interfere in the immunometabolic IDO-1 pathway, as previously described by us[22]. Irinotecan remote loading is accomplished by using ammonium sulfate or sucralose octasulfate for import into the aqueous interiors in the liposome or silicasome, respectively. These trapping agents allow amphipathic weak basic molecules (such as irinotecan, doxorubicin, and mitoxantrone) to cross the LB for protonation inside these carriers, where they collect as slowly dissolving drug precipitates. The hypothesis for the experimentation carried out in this communication is that the generation of immunogenic cell death by irinotecan will be boosted by co-delivery of 3M-052, leading to improved dendritic cell activation. Adapted with permission from ref 15. Copyright 2022 American Chemical Society.

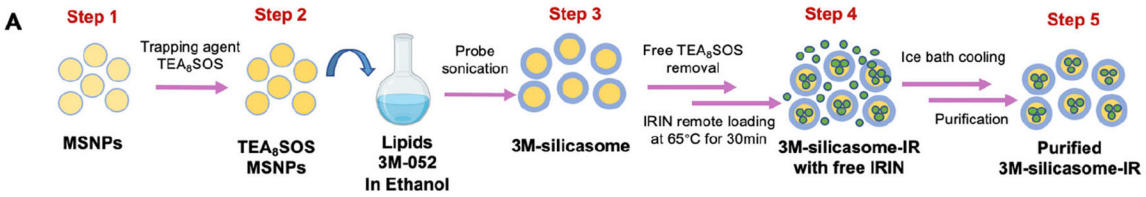

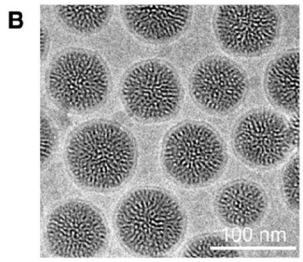

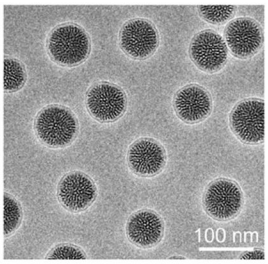

D

Sample	Size (nm)	PDI	Zeta potential (mV)	3M-052 loading capacity (%)	IRIN loading capacity (%)
3M-silicasome	112.2±1.0	0.102	-9.1±0.9	2.1	-
3M-silicasome-IR	127.0±2.9	0.066	-12.8±2.0	1.5	37.9

Figure 2. Development of a co-formulated silicasome drug carrier to deliver a combination of 3M-052, plus the ICD-chemotherapeutic agents IRIN.

(**A)** Schematic to outline the synthesis steps for constructing the silicasome. Briefly, MSNP was soaked in TEA_8SOS trapping agent at 65 °C (step 1), prior to adding to preheated (65 °C) pure ethanol, into which we dissolved a mixture of 3M-052 and lipids (DSPC/Chol/DSPE-PEG2000/3M-052, in the molar ratio of 55.5:38.5:2.7:3.3) (step 2). This mixture was sonicated to provide LB coating (step 3). For IRIN remote loading, irinotecan was dissolved in HEPES-buffered dextrose, before mixing and incubation of the purified TEA_8SOS-loaded 3M-silicasome at 65 °C (step 4). After quenching in ice water, the 3M-silicasome-IR was purified (step 5). As a control, we also synthesized a silicasome that incorporates 3M-052 only, without irinotecan loading (3M-silicasome-IR). CryoEM visualization of the (**B)** 3M-silicasome and (**C)** 3M-silicasome-IR. The bar is 100 nm. **(D)** Physicochemical properties of both silicasomes, including hydrodynamic size, polydispersity index (PDI), zeta potential, and drug loading capacities.

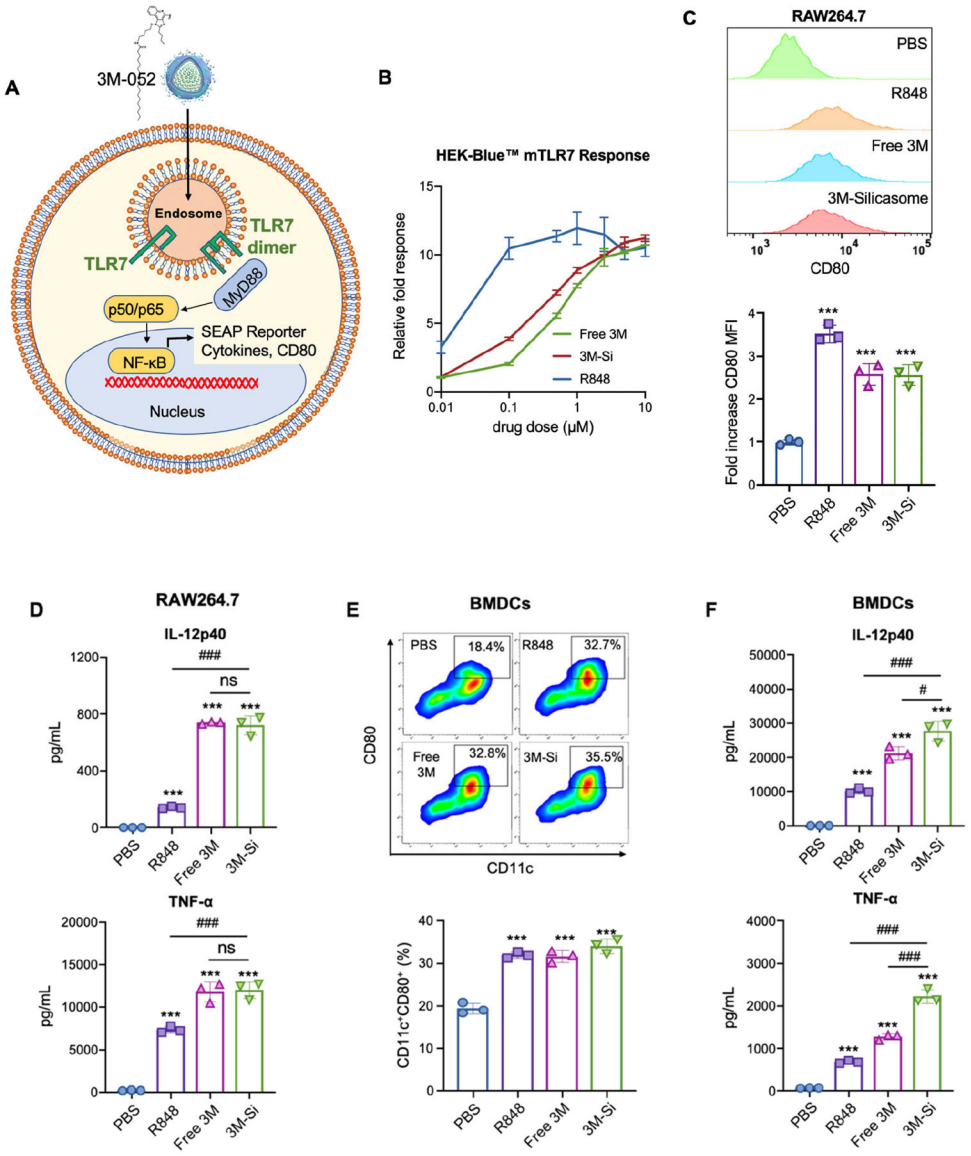

Figure 3. Demonstration of TLR7/8 agonist effect of the 3M-silicasome *in vitro*.

(A) Schematic illustration of the TLR7-mediated signaling pathway, as portrayed for the HEK-Blue™ mTLR7 cell line. **(B)** Dose-dependent (fold) increase in activation of the SEAP transporter gene in HEK-Blue™ cells in response to treatment with a dose range of free R848, free 3M, and 3M-silicasome. (**C**) Flow cytometry analysis to quantify CD80 expression in the RAW264.7 macrophage cell line in response to the same stimuli, used at 10 μM. **(D)** ELISA results in the same cell line for IL-12p40 and TNF-α release in response to 10 μM of the same stimuli. **(E)** Flow cytometry analysis for CD11c expression on BMDCs by the same stimuli. **(F)** ELISA results for the same cytokines in cytokines in BMDCs as for (D). Data represent mean ± SEM, n = 3. ***p < 0.001, $^{\#\#}$p < 0.01, $^{\#\#\#}$p < 0.001.

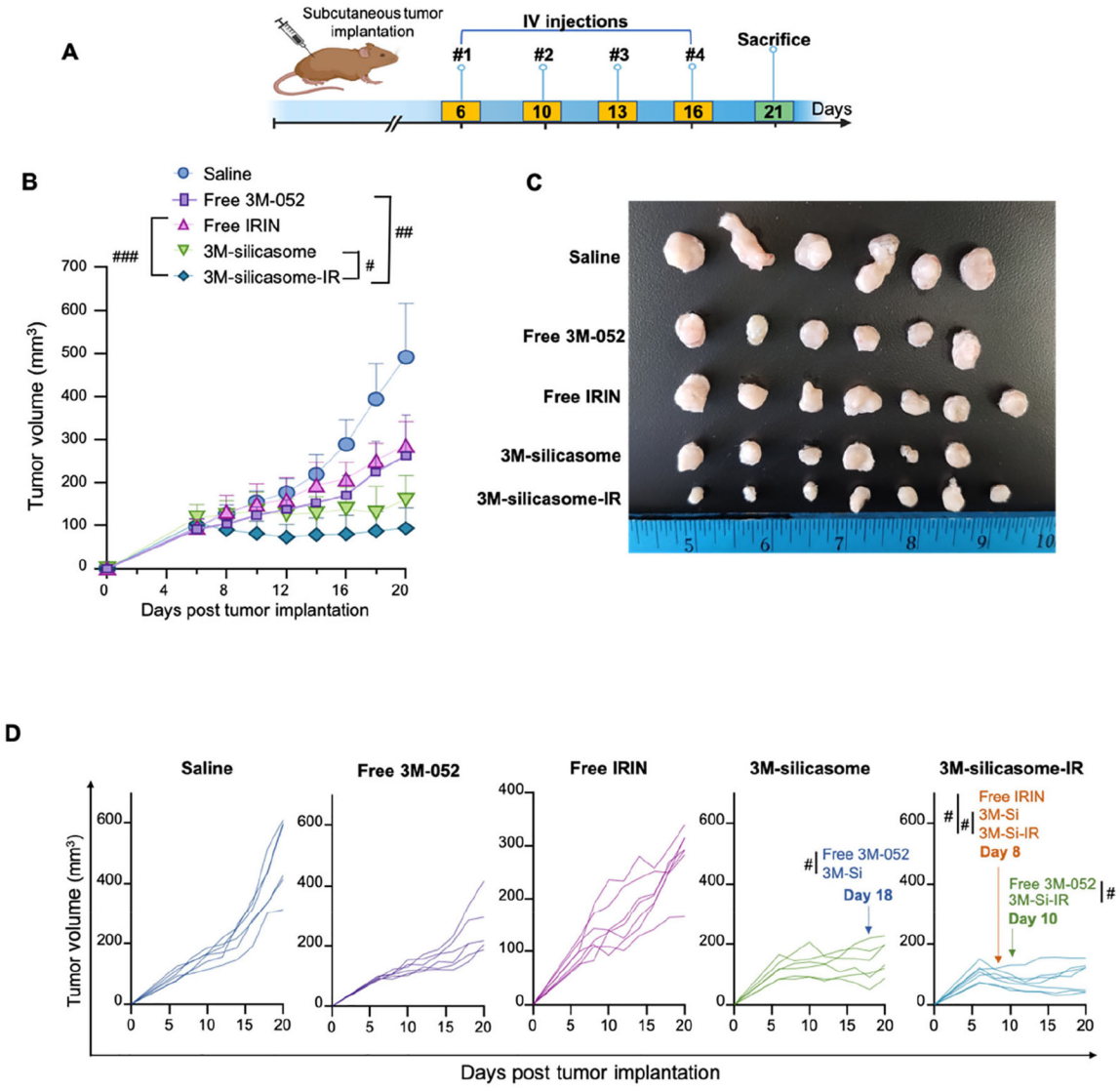

Figure 4. Therapeutic impact on tumor growth in a subcutaneous KPC model.

(**A)** Experimental timeline to assess the therapeutic impact of single and dual delivery carriers in subcutaneous KPC tumor-bearing mice. (**B)** Averaged tumor growth kinetics (n=6–7) through assessment of tumor volume in animals treated with saline, free 3M-052, free IRIN, 3M-silicasome, and 3M-silicasome-IR at dose equivalents of 2 mg/kg and 40 mg/kg for 3M-052 and IRIN, respectively, every 3–4 days, for a total of 4 IV injections. Please notice that the inhibition of tumor growth by free 3M-052, free IRIN, 3M-silicasome, and 3M-silicasome-IR is statistically significant compared to the saline control ($p<0.001$) on day 20. Although limited animal availability during COVID-19 precluded the inclusion of a carrier delivering encapsulated IRIN only, we have previously shown the advantage of an IRIN silicasome over liposomal or free drug delivery in KPC tumors.[7–9] **(C)** photographic images of harvested tumors at the same magnification on day 21. (**D)**. Spaghetti plots to depict the individual tumor growth kinetics over the course of the study. These plots further depict that inhibition of tumor growth by 3M-silicasome becomes statistically significant

compared to free 3M-052 ($p<0.05$), from day 18 onwards. Moreover, inhibition of tumor growth by 3M-silicasome-IR becomes statistically significant from free IRIN and the 3M-silicasome ($p<0.01$) from day 8 onwards, and from free 3M-052 ($p<0.01$) from day 10 onwards. Data represent mean ± SEM. $^{\#}p < 0.05$, $^{\#\#}p < 0.01$, $^{\#\#\#}p < 0.001$.

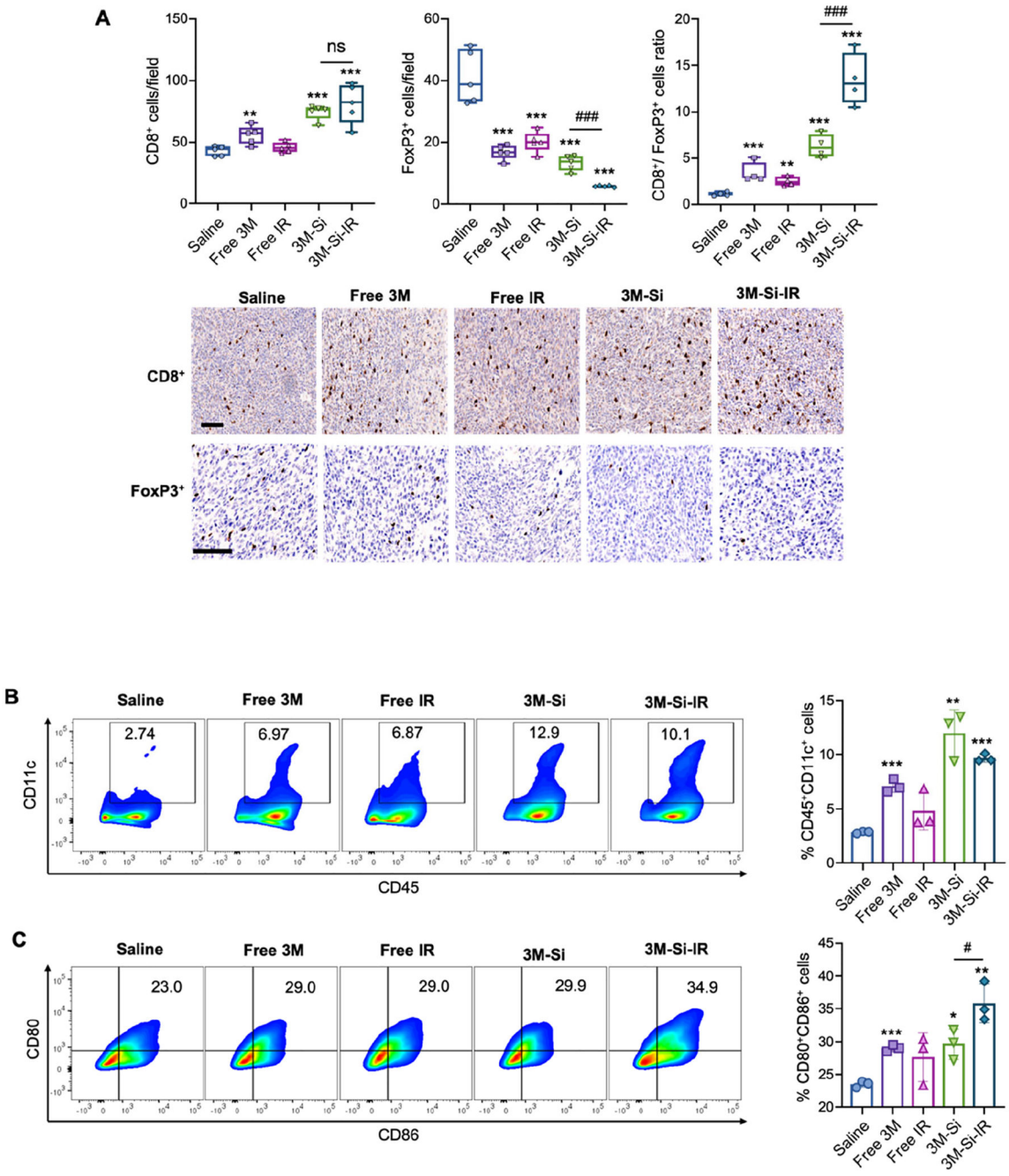

Figure 5. Evidence of therapeutic anti-PDAC immunity in the subcutaneous pancreatic cancer model.

KPC tumor-bearing mice were euthanized on day 21, followed by harvesting of the primary tumors and regional draining inguinal lymph nodes. (**A)** Representative IHC images and the quantification of $CD8^+$ and $FoxP3^+$ cell numbers at the primary tumor sites of different animal groups. 5 primary tumors in each group were analyzed. 3 fields were randomly selected for counting and the average cell number in each mouse was shown in the graphics. Bar is 100 μm. Data represent mean ± SEM. (**B)** Representative flow cytometric analysis for quantitation of CD45+ dendritic cells in the lymph nodes, using the gating procedure

described in online Figure S6. **(C)** Flow cytometry analysis of the percentage $CD80^+CD86^+$ cells in $CD11c^+/CD45^+$ population. Data represent mean ± SEM, *p < 0.05; **p < 0.01; ***p < 0.001, $^{\#\#\#}p < 0.001$.

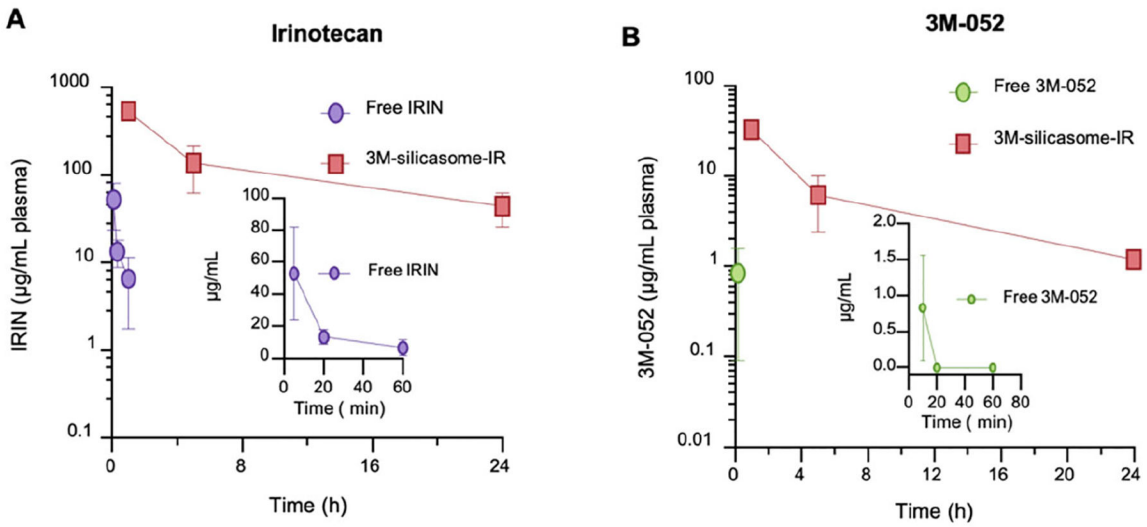

Figure 6. Pharmacokinetics and drug delivery by silicasomes versus free drugs.

Healthy B6129SF1/J mice received one IV injection of free 3M-052, free IRIN, and 3M-silicasome-IR at dose equivalents of 2 mg/kg and 40 mg/kg for 3M-052 and IRIN, respectively. Blood collection was performed at 1, 5, 24, and 48 h post-injection (n=3). Free 3M-052 and IRIN were extracted by methanol, and plasma drug concentrations were measured by HPLC, as described in the experimental section. While free IRIN (panel **A**) and free 3M-052 (panel **B**) rapidly disappeared from the blood (i.e., < 60 min, prompting the inserted graphs display), the 3M-silicasome-IR significantly increased both plasma IRIN and 3M-052 concentrations.

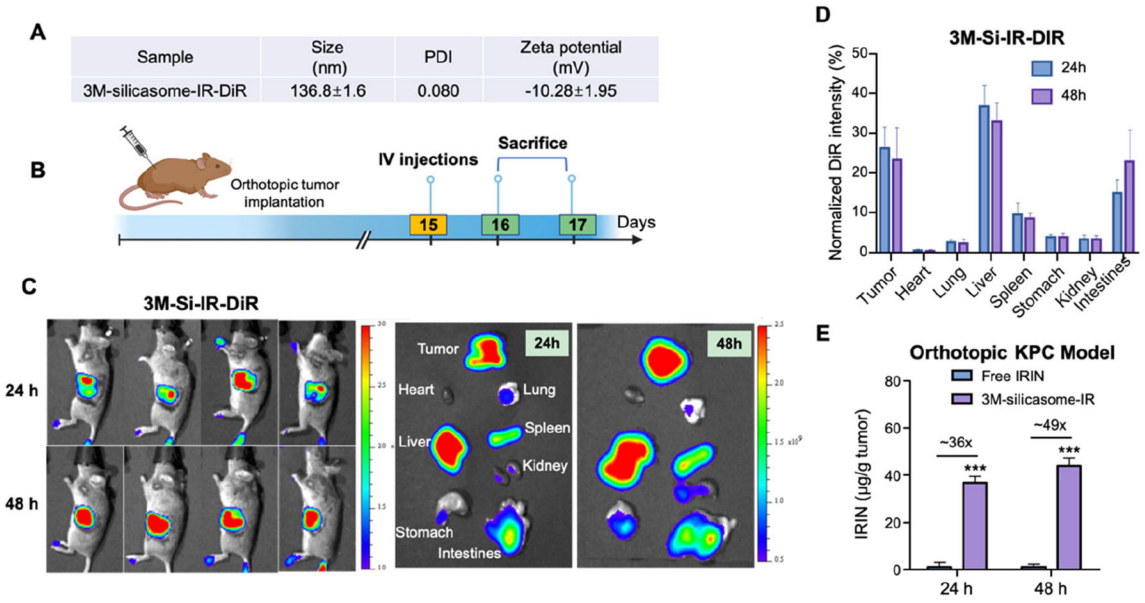

Figure 7. Use of DiR-labeled dual-drug silicasomes to assess *in vivo* biodistribution in an orthotopic KPC model.

A DiR-labeled 3M-silicasome-IR nanocarrier was prepared for biodistribution assessment in an established KPC-derived orthotopic tumor model in B6129SF1/J mouse model. Tumor-bearing mice received one IV injection of saline, free IRIN, and DiR-3M-silicasome-IR at a dose equivalent of 40 mg/kg for IRIN. The *in vivo* and *ex vivo* IVIS imaging in the DiR label group were performed 24 and 48 h after IV injection, as well tumors were collected from all groups to determine IRIN contents by HPLC analysis. **(A)** Physicochemical properties of the DiR-labeled3M-silicasome-IR, including hydrodynamic size, PDI, and zeta potential. **(B)** Experimental timeline for the drug biodistribution study in orthotopic KPC tumor-bearing mice (n=3 or 4 animals). (**C)** *In vivo* and *ex vivo* fluorescence imaging and B6129SF1/J mice, 24 and 48 h after IV particle injection. The *ex vivo* IVIS image is representative of one of the animals in each of the 24 and 48 h animal groups. Additional *ex vivo* images appear online in Figure S7. (**D)** Normalized fluorescence intensities, expressed as radiant efficiency, were calculated for all the explanted organs 24 and 48 h after IV injection. (**E)** The IRIN contents at the primary tumor sites were determined by HPLC analysis, as described in the experimental section. Data represent mean ± SEM. ***p < 0.001.

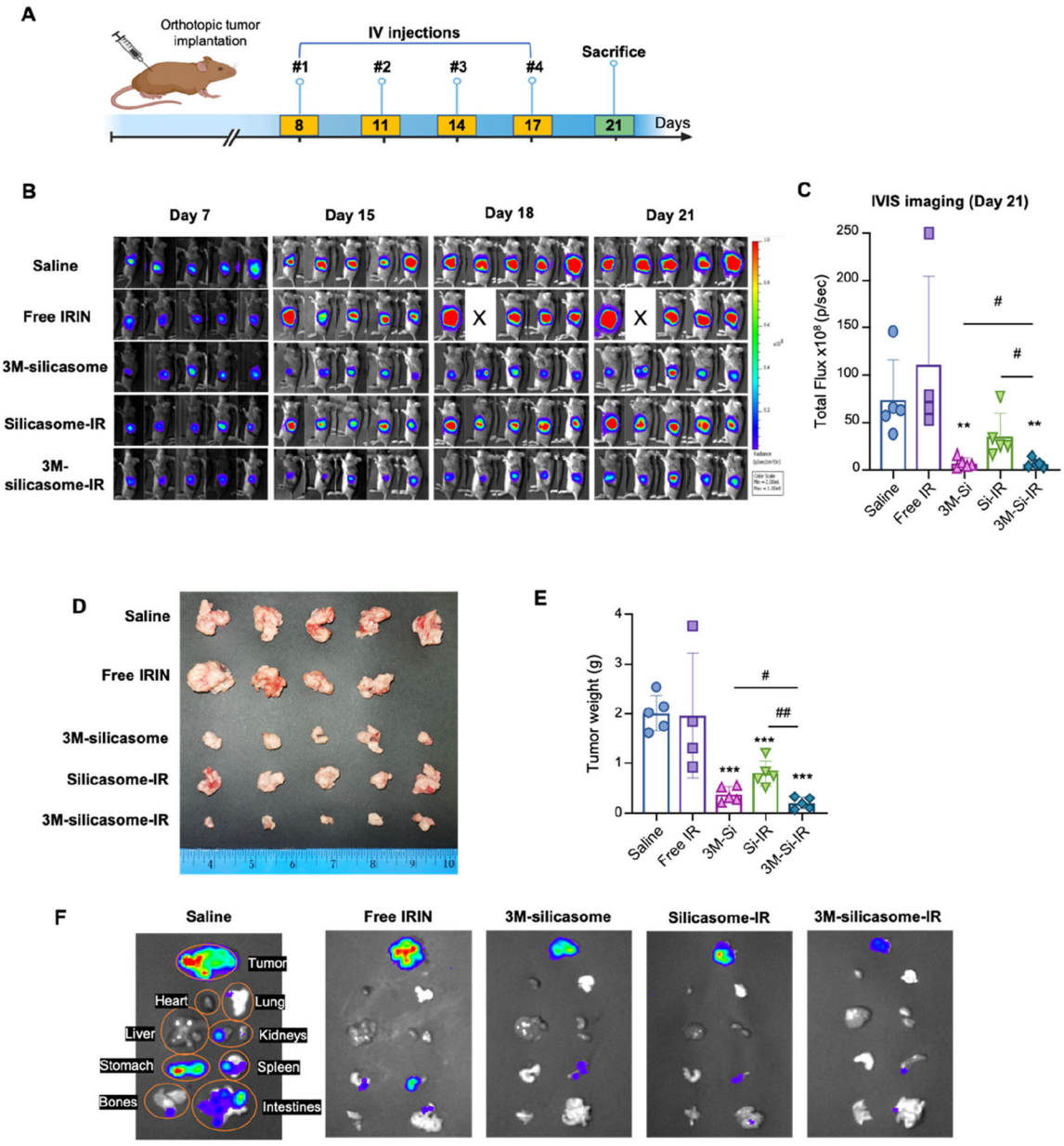

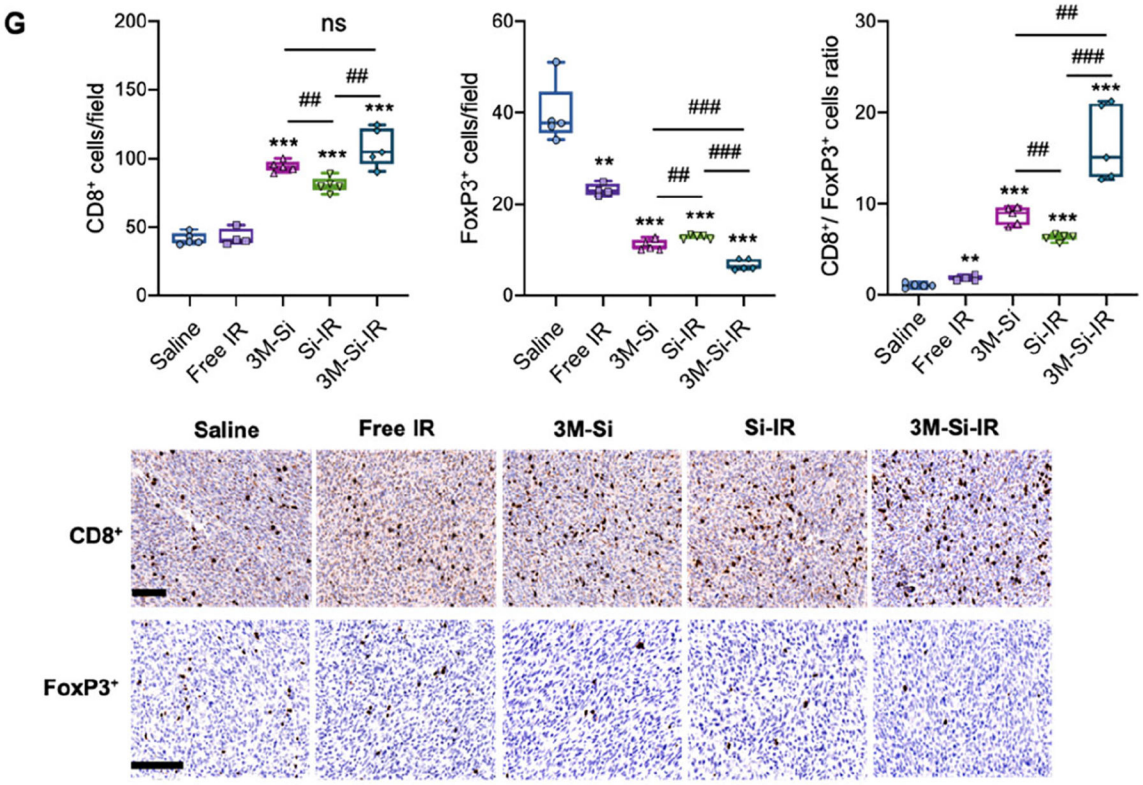

Figure 8. Demonstration of synergistic drug effects in an orthotopic pancreatic cancer model.

(**A)** Experimental timeline for tumor inhibition in orthotopic KPC tumor-bearing mice (n=5). (**B)** IVIS images of individual tumors in each treatment group were obtained on days 7, 15, 18, and 21. **(C)** Use of IVIS software to calculate the average tumor bioluminescence intensity for each group on day 21. (**D)** Photographs and calculation of (**E)** average primary tumor weights in each group were obtained on day 21. (**F)** *Ex vivo* IVIS imaging of explanted organs from the orthotopic tumor-bearing mice were obtained on day 21. (**G)** Representative IHC images and the quantification of $CD8^+$ and $FoxP3^+$ cell numbers in the different treatment groups. 4 to 5 primary tumors in each group were analyzed. 3 fields were randomly selected for counting and the average counting number in each mouse was shown in the graphics. Bar is 100 μm. Data represent mean ± SEM. $^{**}p < 0.01$; $^{***}p < 0.001$, $^{\#}p < 0.05$, $^{\#\#}p < 0.01$, $^{\#\#\#}p < 0.001$.